Controlling vapor-liquid-solid growth of copper-seeded silicon microwire arrays for solar fuel generation

by

Sridhar Majety

A Thesis submitted to the Faculty of Graduate Studies of

The University of Manitoba

in partial fulfillment of the degree of

MASTER OF SCIENCE

in the

Faculty of Engineering

Department of Electrical and Computer Engineering

Acknowledgements

I would like to thank the Department of Electrical and Computer engineering for accepting me to the master's program. I am greatly indebted to my advisor Prof. Derek Oliver for his inspiration and support, as well as encouragement to pursue ideas and shaping them with his valuable critique. I am thankful to Prof. David Herbert for allowing me to access the microwire growth facility in the Department of Chemistry. My research work wouldn't have been a better experience without the support of my colleagues Onkar Singh Kang, Patrick Giesbrecht, Kevin McEleney, Ravinder Sandhu, Jordan Engel, Alex Ogaranko, Seth Cathers and Tao Xu. I would like to thank my family who supported my decision to pursue graduate studies and my friends Emily Barker, Praneeth Chakravarthula, Venkata Revanth for talking me out of my frustrations. And to my other friends in engineering Mrigank Rochan, Mallikarjun Thammiah, Sumanth Kuntavalli, Puneet Anand, Vaibhav Dubey, Mayank Thacker, Anton Vykhodtsev for making this entire experience memorable.

Contents

List of Figures

List of Copyright Material obtained with permission

Figure 2-2 Copyright (2009) Macmillan Publishers Ltd: Nature Chemistry.

Figure 2-6 Copyright (2009) Wiley-VCH Verlag GmbH & Co. KGaA, Weinheim.

Figure 2-7 Copyright (2005) American Institute of Physics.

Figure 2-8 Copyright (1975) North-Holland Publishing Company

Figure 2-9 Copyright (2006) American Physical Society.

Figure 2-10 Copyright (2011) Materials Research Society.

Figure 2-11 Copyright (2009) Wiley-VCH Verlag GmbH & Co. KGaA, Weinheim.

Figure 2-12 Copyright (1986) Elsevier B. V.

1 Introduction

The increasing population of the world is resulting in growing need of energy and the energy per capita has been going up too. The world population is 7.6 billion in 2017 and is expected to reach 9.8 billion by 2050 [1]. Over 85% of the current world energy requirements are met through non-renewable sources of energy like coal, oil and natural gas. The possibility of the depletion of crude oil in the near future in combination with the increased greenhouse gas emissions leading to global warming in the past few decades, has motivated mankind to switch towards clean and renewable form of energy.

Renewable energy (excluding hydroelectric energy) production has seen an increase in the last few years and most of it coming from wind energy. Sunlight that is incident on earth surface (1367 W per m^2) is enough to provide the earth with a clean, sustainable form of energy. When the sunlight is incident on a material, photons are absorbed to generate free electrons that contribute to electricity. This phenomenon called the photovoltaic effect led to construction of the solar cell. However, there are problems associated with adoption of solar energy that include the rather poor conversion efficiencies, the storage of the energy, the cost of installation and the variation in the sunlight levels throughout the year. There have been more and more studies to solve the economic and efficiency aspect of the solar devices. Efficient storage of the converted solar energy can address the lack of consistency in the sunlight levels. The solar energy absorbed can be used to produce chemical fuels like hydrogen or the electricity could be used to charge batteries. The chemical fuels or batteries could be used as sources of energy for various purposes.

1.1 Artificial Photosynthesis devices

Photosynthesis refers to the process in which plants use sunlight to convert carbon dioxide and water to sugars and oxygen. The artificial photosynthesis device uses semiconductor material to absorb the sunlight and to split the water molecule into hydrogen and oxygen. The splitting of water molecule happens through the following reaction

$$H_2O \rightarrow H_2 + {}^1/_2\, O_2$$

The hydrogen produced is stored and used as fuel. Combustion of hydrogen releases energy and the only by-product of this process is pure water. It does not involve any carbon emissions and thus may be seen as a potential chemical fuel. The energy required to split a water molecule is 1.23 eV [2] and this energy is provided by the sunlight in these devices. The splitting of water molecules involves losses such as inefficiencies in electron transfer at semiconductor/electrolyte interface and resistive losses in the microwires arrays. Thus the energy required for successfully splitting water can vary between 1.6-2.4 eV [2]. The requirement for a material to successfully split water molecule is that the conduction and valence band of the material should straddle the electrochemical potential of hydrogen evolution reaction and oxygen evolution reaction. A water splitting cell has been demonstrated using TiO_2 [3] which has a bandgap of 3.2 eV. However, using materials with bandgap > 2 eV would be inefficient because of poor conversion efficiencies [4].

Silicon, with a bandgap of 1.15 eV, is a suitable material for a single bandgap solar cell with good conversion efficiencies. However, smaller band gap materials need to be used in combination with other smaller bandgap materials to carry out the water splitting reaction [2]. A dual bandgap configuration also allows the possibility to have separate half cells for hydrogen and oxygen evolution reactions, which makes collection of the byproducts more efficient. High aspect ratio

microwire structures have been used to obtain better carrier collection efficiencies, which are grown using a Vapor-Liquid-Solid method. Differently doped microwires can be grown using this method. The doping levels are chosen such that the conduction band on the hydrogen evolution side and the valence band on the oxygen evolution side straddle the electrochemical potentials required for hydrogen evolution reaction and oxygen evolution reaction. The microwires grown using this method have sidewall properties that are based on the growth conditions chosen and are critical for attaching catalysts onto the surface of the microwires. This improves the carrier transfer at the semiconductor/electrolyte interfaces. The purpose of this project is to set out the growth parameters to grow p-n or p-i-n microwires that will enable efficient water splitting using sunlight.

1.2 Thesis Outline

The following parts of the thesis is divided into four chapters. The second chapter- literature review, covers the theoretical background required for this research work that is covered by the thesis. The chapter starts with an introduction to the cell configurations for the artificial photosynthesis device and the requirements of the semiconductor material for the implementation of such a device. This is followed by an overview of the Vapor-Liquid-Solid (VLS) method- the growth process for high aspect ratio microwires. The following sections of the chapter mainly covers the requirements of the catalyst materials for the VLS growth process and the role of temperature, carrier gas, precursor gases and doping mechanism in microwire growth.

The third chapter starts with the cleanroom fabrication procedure to pattern the silicon substrate with the copper catalyst. This is followed by a description of the chemical vapor deposition furnace used for VLS growth. A range of growth conditions for microwires have been used to understand the impact of silicon precursor and dopant gas flowrates on microwire properties. In the second half of this chapter, the procedure to isolate microwires from the growth substrates is described.

The microwires are put onto a glass slide to perform two-point and four-point electrical measurements. These electrical measurements are used to calculate the doping concentrations for various growth conditions used in this study.

The fourth chapter involves the results and discussions of the study. In the initial part of this section an understanding of the impact of silicon precursor and dopant gas flow rates on the dopant concentration is presented through a detailed discussion of the microwires using four-point electrical measurements. The impact of the catalyst as a dopant in the microwires is also discussed. In the next part of this section an understanding the impact of the silicon precursor and dopant gas flowrate on the sidewall properties of the microwires is obtained by examining the scanning electron microscope (SEM) images of the microwires. Towards the end of the chapter, composite microwires with varying silicon precursor flowrates in a single growth run and microwires grown with two differently doped regions are examined.

In the final chapter a conclusion of the study and future work are presented. This section lists the direction of research that needs to follow the work done in this thesis.

2 Literature Review and Theory:

The photo-electrolysis process involves conversion of light energy into electrical energy. This electrical energy is utilized to split the water molecule into hydrogen and oxygen, in the case of a water splitting cell. A single molecule of water splits according to the reaction:

$$H_2O \rightarrow {}^{1}/_{2}\, O_2 + H_2 \qquad \Delta G = +237.2\ kJ.mol^{-1}$$

$$2H^+ + 2e^- \rightarrow H_2 \qquad \text{Hydrogen Evolution Reaction}$$

$$H_2O + 2h^+ \rightarrow {}^{1}/_{2}\, O_2 + 2H^+ \qquad \text{Oxygen Evolution Reaction}$$

The free energy change (ΔG) to convert one molecule of water to H_2 and ½ O_2 under standard temperature and pressure (STP) conditions (273 K and 760 Torr respectively) is 237.2 kJ/mol. The corresponding to an electro-chemical potential difference, $\Delta E^o = 1.23$ eV, is the energy transferred per electron [2], [5].

The idea of a solar water splitting cell could be realized by using semiconductor materials, which absorb solar energy to generate the carriers (electrons/holes) which in turn drive the water splitting reaction. The ideal semiconductor material to carry out a water splitting reaction should have a bandgap (E_g) large enough to split water (E_g>1.23 eV). Also, the conduction band edge (E_{cb}) and the valence band edge (E_{vb}) straddling the electrochemical potentials $E^o(H^+/H_2)$ and $E^o(O_2/H_2O)$ i.e., the conduction band energy (E_{cb}) should be higher than the electrochemical potential for hydrogen evolution- $E^o(H^+/H_2)$ and the valence band energy (E_{vb}) should be lower than the electrochemical potential for oxygen evolution- $E^o(O_2/H_2O)$ as shown in figure 2-1. Under illumination, electrons and holes with energies sufficient to drive the hydrogen evolution reaction (HER) and oxygen evolution reaction (OER) are generated.

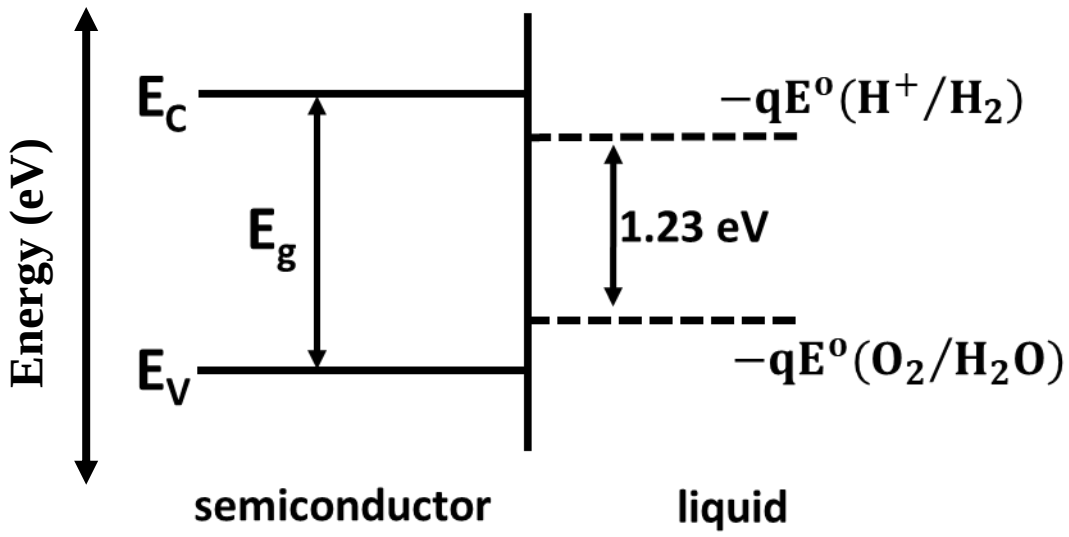

Figure 2-1 The conduction (E_C) and valence (E_V) bands of an ideal semiconductor for a water splitting reaction with absolute energy scale on the left axis.

The carriers generated by the absorption of light energy need to travel to the semiconductor surface before recombination, to participate in the electrolysis half-reaction. The carrier recombination is determined by the minority carrier diffusion length (L_D), the average distance a minority carrier diffuses before recombination. In a bulk semiconductor, to be able to collect carriers efficiently, $L_D > 1/\alpha$ (absorption length), where α is the absorption co-efficient of semiconductor material near its bandgap energy (E_g). Structures with high aspect ratio and larger surface area (for example: non-planar structures like micro/nanowires), reduce the distance travelled by the carriers to reach the surface (radially), while the light is still being absorbed along the length of the wire (axially). Thus, this decoupled L_D from absorption length and allows high carrier collection efficiencies [6], [7]. The carriers reaching the surface are transferred at the semiconductor/electrolyte junction to drive the OER and HER. The transfer process involves losses related to electron transfer at semiconductor/electrolyte interface and resistive losses in the microwires arrays. Taking into

account all such losses, the energy required for photo-electrolysis at a semiconductor electrode is reported to be between 1.6-2.4 eV per electron-hole pair generated [8], [9].

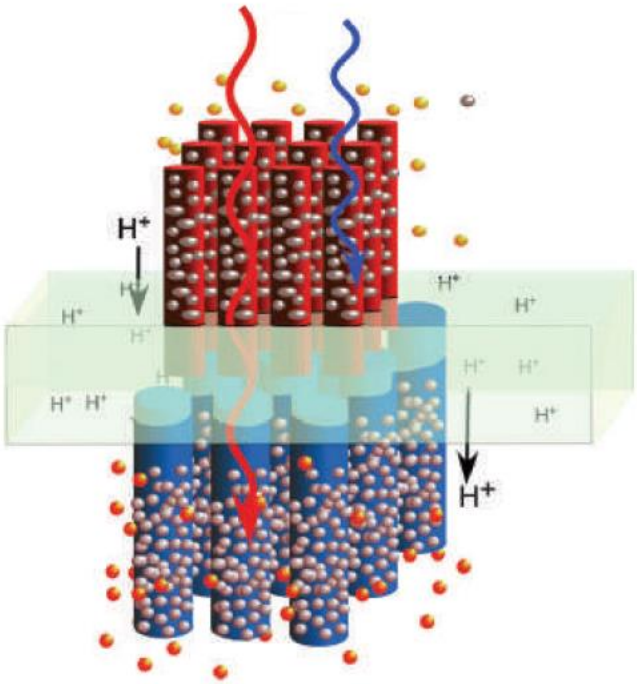

Figure 2-2 Prototype device proposed by Gray [10] with high aspect ratio structures as the photo-electrodes. The red region is n-type material- to carry out the oxidation of water and the blue region is p-type material- to carry out proton reduction. The green region is an ionic membrane that allows conduction of ions and electrons between the two regions. The spheres on the surface of these high aspect ratio structures represent a catalyst to promote the OER and HER. Reprinted with permission from [10]. Copyright (2009) Macmillan Publishers Ltd: Nature Chemistry.

A single bandgap device could be used for water splitting but for bandgaps larger than 2 eV the maximum theoretical efficiencies of these cells drop drastically. A solution to this problem was to use multiple bandgap cells with smaller bandgap semiconductor materials. Such a dual bandgap configuration in a water splitting device would allow separation of the OER and HER thus enabling safe and efficient collection of oxygen and hydrogen. Silicon is an attractive candidate as semiconductor material for water splitting applications because it is earth-abundant and ubiquitous

in the technology industry. The bandgap of 1.12 eV for p-type silicon is suitable for splitting water in a dual bandgap configuration for hydrogen evolution.

Prototype devices using semiconductor electrodes to absorb sunlight and store it in the chemical bond of hydrogen via water splitting are of growing interest. Gray's proposal [10] for such a system consisted of two sets of microwires, p-type (photoanode) and n-type (photocathode) connected in series through a conducting polymer membrane. This cell could safely separate the oxygen-evolving and hydrogen-evolving half-cell reactions associated with the water splitting (see Figure 2-2 in [10]). In such a dual bandgap configuration, the bandgaps of both the electrodes must be appropriate to produce enough photovoltage to drive both the HER and OER.

In principle, a single p-i-n microwire structure with the conducting polymer membrane positioned across the intrinsic region is an alternative to the conventional two wire and membrane structure (Figure 2-3). Aside from reducing some of the design requirements for the conducting polymer membrane, the intrinsic region would reduce the leakage current losses along with any losses due to contact resistance of microwire/membrane system.

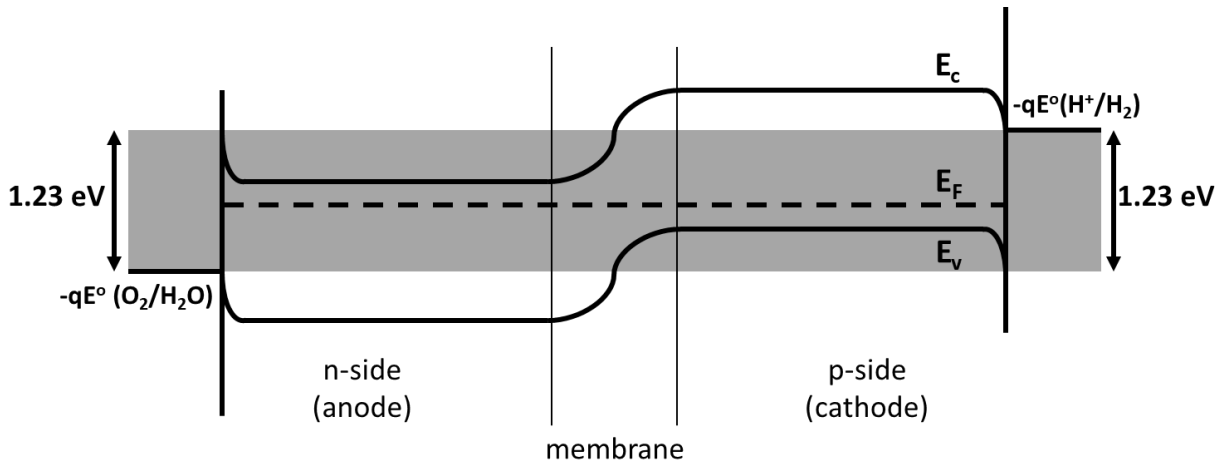

Figure 2-3 p-i-n microwire structure shown with energy band diagrams straddling the electrochemical potentials of OER and HER required for splitting of water into hydrogen and oxygen.

2.1 Silicon microwire arrays grown using Vapor-Liquid-Solid (VLS) technique:

The vapor-liquid-solid (VLS) mechanism is a chemical vapor deposition (CVD) process which allows a bottom-up synthesis of highly crystalline silicon (or any other material) wires. The mechanism for growing silicon whiskers using VLS was first proposed by Wagner and Ellis [11] in 1964. The observations made in their study were:

1. The whiskers are dislocation free and unidirectional (mainly growing in the <111> direction).
2. Impurities are essential for the whisker growth.
3. A liquid-like globule is located at the tip of the whiskers during their growth. The extension in length of the whisker occurs by addition of material to this globule at the tip.

When gold is deposited onto a silicon substrate and then heated to temperatures above 363 ºC, droplets of a Au-Si alloy will form on the surface. When this alloy droplet is exposed to silicon precursor gases like silicon tetrachloride ($SiCl_4$) or silane (SiH_4) the gas molecules dissociate on the surface of the droplets and the silicon then gets incorporated into the droplet. The continued supply of silicon to the droplet make it supersaturated with silicon, resulting in silicon crystallizing at the droplet/silicon substrate interface. The vapor silicon is dissolved in the droplet, passes through it and finally deposits as a solid. Hence the name vapor-liquid-solid (VLS) for this growth mechanism.

The wires grown in this process can be doped by using doping precursors. By switching the dopant gas and its flowrate the doping profile of the wire can be varied in the axial direction. The benefit of the VLS process is that it allows for a wide range of diameters for the liquid droplet, from tens

of nanometers to hundreds of micrometers. The growth rate of the wires is an important parameter to understand and is dependent on the diameter of the droplet. The radius dependence of growth rate depends on the rate determining step of the VLS growth process.

The VLS process involves three phases and two interfaces (vapor-liquid, liquid-solid). The choice of the growth conditions decides the rate determining step. The process occurs in four main steps (figure 2-4):

1. Mass transport of the precursors in the gas phase
2. Incorporation step: silicon precursor cracks at the surface of the droplet and silicon is incorporated into the droplet.
3. Diffusion step: dissolved silicon atoms diffuse from the vapor-liquid interface to the vapor-solid interface.
4. Crystallization step: silicon crystallizes at the liquid-solid interface to form a silicon wire.

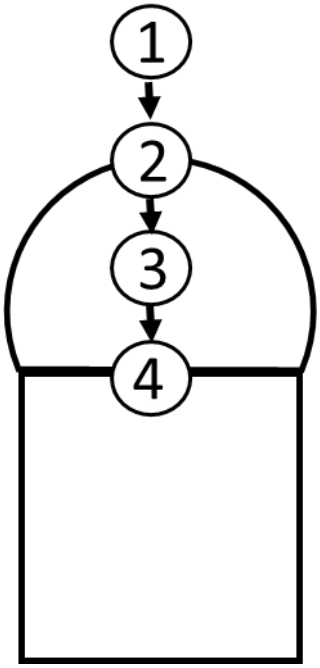

Figure 2-4 Schematic indicating the interfaces at which the 4 steps of a VLS process occur.

The kinetic coefficients for the VLS process are an exponential function of temperature, whereas the mass transport in gas phase usually follows a power law [12]. Thus, step 1 has no role in determining the growth rate. The droplet is almost a hemisphere and thus the diffusion length from the vapor-liquid interface to the liquid-solid interface is a function of the thickness of the whiskers. The observation that the rate of growth is independent of whisker thickness [12] suggest that step 3 can also be neglected when determining the growth rate.

Bootsma and Gassen [13] concluded that the incorporation step is the rate determining step based on the observation that the growth rate of silicon and germanium whiskers is linearly proportional to the partial pressure of their precursors (SiH_4 and GeH_4). However, Givargizov [12] argued in favor of the crystallization step being the rate determining step, based on the observation that growth rate depends on the crystallographic direction in grown GaAs whiskers. However, the conflict can be resolved by replacing the assumption of a single rate determining step with an interplay between the incorporation and crystallization steps to determine the growth rate [14].

The critical parameter in determining the growth rate is the supersaturation of the droplet, which is defined by the silicon chemical potential difference in the droplet and the nanowire [14]. If there isn't sufficient supersaturation of the droplet, the crystallization and hence the growth of the wire does not happen. As the droplet becomes more supersaturated, the crystallization rate increases and silicon chemical potential difference between the droplet and the silicon vapor decreases i.e., incorporation rate reduces. Under steady-state growth conditions, the incorporation rate should be equal to the crystallization rate. The steady state condition determines the supersaturation in the droplet to levels at which the incorporation and crystallization rates are equal. It can be concluded

that, the growth rate is an interplay of both incorporation and crystallization steps. Some other possible growth mechanisms are discussed in section 2.3.

2.2 Catalyst Materials for VLS growth:

In some of the initial work for silicon whisker growth [11] gold was used as a catalyst material to grow silicon whiskers through VLS mechanism. Most of the research involving VLS growth of microwires or nanowires involved the use of gold as the catalyst. The several advantages gold offered were:

1. Gold was one of the standard metals used for electrical contacts and hence was available in most of the evaporation systems.
2. Gold has a high chemical stability and doesn't oxidize easily even at elevated temperatures. Thus, reducing the constraints on the oxygen background pressure.
3. The gold-silicon eutectic system has a strong reduction in the melting point (eutectic point=363 ºC) in comparison to the individual melting points of gold (1064 ºC) and silicon (1414 ºC).
4. High % of silicon at eutectic point as shown in the phase diagram (Figure 2-5) indicates a high solubility of silicon in the eutectic mixture. Thus, offering good growth rates and allowing low silicon precursor partial pressures with which to work.
5. Gold has low vapor pressure at elevated temperatures (less than 10^{-8} mbar at 800 ºC). Hence, there is no loss of metal catalyst through unwanted evaporation during growth.

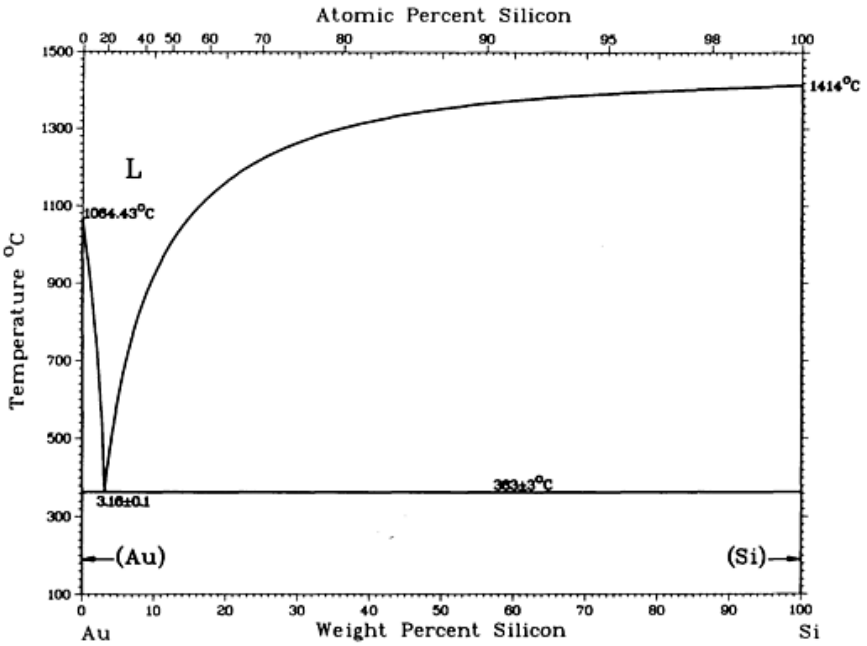

Figure 2-5 Gold-silicon system phase diagram [15].

However, the biggest disadvantage for gold is that it is not compatible with complementary metal-oxide-semiconductor (CMOS) production standards as it creates an impurity level in silicon close to the center of the bandgap. This acts as a very efficient recombination center, significantly reducing carrier lifetimes. The high chemical stability of gold inhibits removal of contaminant atoms. These reasons motivated studies of alternate catalyst materials for silicon whisker growth. All metals cannot be catalysts for VLS growth of silicon whiskers and the requirements for VLS growth catalysts are [16, Ch. 1]:

1. It must have the ability to form a eutectic mixture (liquid) with silicon (for this research).
2. The solubility limit of the metal in liquid phase (C_l) must be higher than that in the solid phase (C_s) i.e. $K=C_s/C_l < 1$. This condition ensures minimal contamination of the whisker grown and also prevents the reduction of the droplet volume (thus the wire cross-section) during growth.

3. The vapor pressure of the metal at elevated temperatures should be small compared to the pressure in the chamber during growth. This prevents metal the loss of metal catalyst through evaporation.
4. The metal needs to be inert to chemical reactions. Any reaction of the metal with the precursor gases could hamper the catalytic nature of the metal.
5. The surface tension of the liquid droplet should fulfill the Nebol'sin stability criterion [17] as defined below.

A range of alternative metals have been explored based on the type of whiskers grown e.g. copper [17]–[20], aluminium [17], [21], [22], silver [17], [23]–[25], nickel [12], [17], [26], [27], platinum [12], [17], [26], [28], zinc [17], [26], [29]. The behavior of various metals as a dopant in the whisker is discussed in the further sections.

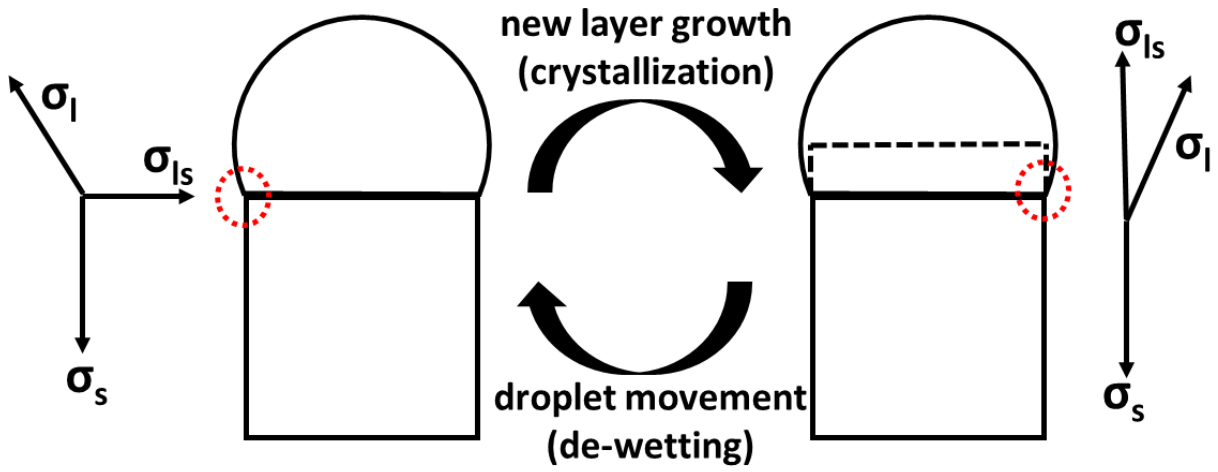

Figure 2-6 Silicon whisker growth as a cycle of two steps: crystallization, droplet movement. The forces acting at the edge of the liquid-solid interface (red circle) are shown for both the cases. The newly grown layer is indicated by a dashed line. Adapted with permission from [14]. Copyright (2009) Wiley-VCH Verlag GmbH & Co. KGaA, Weinheim.

In the VLS mechanism, after the crystallization step and formation of a layer of silicon, the metal droplet wets the sidewall of the whisker. This would result in a net vertical force that pulls the droplet upwards by an amount equal to thickness of the newly grown layer i.e. the droplet de-wets the sidewall of new layer. The continuous cycle of crystallization (wetting) and de-wetting results in the silicon whisker growth as is shown in Figure 2-6. To have a stable and continuous growth, the net force in the vertical direction must be upwards, which puts a lower limit on the surface tension of the liquid. The Nebol'sin stability criterion determines the relationship between the surface tension of the liquid (σ_l) and the surface tension of the solid (σ_s) for a net upward force to exist, and to de-wet the sidewall is given as:

$$\sigma_l > \sigma_s/\sqrt{2} \qquad (1)$$

where σ_l is the surface tension of the liquid and σ_s is the surface tension of the solid. The value of σ_s for silicon is 1.2 J m^{-2} [17] and this puts a lower limit on σ_l of about 0.85 J m^{-2}. Droplets with surface tension lower than this value are not capable of de-wetting the sidewall. Metals exhibit a range of surface tension values: copper, nickel, platinum have surface tension values > 1.3 J m^{-2}; silver and gold have values closer to 0.9 J m^{-2}; while for aluminum, the value is 0.8 J m^{-2}. Metals with lower surface tension values (e.g. bismuth, lead and antimony have values around σ_s = 0.4 J m^{-2} [17], [30]–[32]) tend not to promote whisker growth [17], although indium (0.5 J m^{-2} [17]) has been an effective VLS catalyst [17], [33], [34].

2.3 Parameters involved in growth

The VLS process is a chemical vapor deposition method in which precursor gases are flowed into a chamber holding a substrate coated with metal catalyst and heated to temperatures above the

eutectic temperature of the metal-silicon system. The growth process and the resulting microwire properties are influenced by the temperature, the pressure, the metal catalyst, the diameter of the wire, the nature of gases involved. The identifiable influences of each of these parameters are discussed in the following subsections.

It has been observed that the silicon wires grown using this process are enlarged in the region where the wire is connected to the substrate [35]. This expansion at the base should not be looked on as an overgrowth of silicon. Givargizov [36] found that the expansion at the wire base is independent or a weak function of the growth temperature used and the shape of the expansion roughly scales with the diameter of the wires grown. Based on which he concluded that the expansion of the base is related to a change in the contact angle of the droplet and not due to overgrowth.

When the substrate is heated, a liquid alloy droplet is formed, and the shape of this droplet determined by the liquid-solid contact angle, depends on the rate at which temperature increases during alloying [35]. Gold-silicon alloy droplets showed a contact angle of 43º on flat silicon surfaces, in the temperature range 400-650 ºC [37]. As the wire starts to grow, the contact angle increases and as a result the diameter of the wire decreases gradually. Once the wire grows beyond the tapered section, the contact angle stabilizes and remains constant (no change in diameter) if the growth temperature is not changed. It was observed that the droplet on top of a wire has a contact angle close to 120º [38]. Evidently, the droplet shape and contact angle have to transition in the initial stages of growth and thus validating Givargizov's [36] conclusions. Qualitative models were also derived based on Givargizov's explanations which agreed with the experimental observations [39].

2.3.1 The role of temperature

The catalyst-silicon system should be heated to temperatures above eutectic temperature to form a liquid alloy. When the temperature is increased above the eutectic temperature, the solubility of silicon in the droplet increases and thus reduces the supersaturation and the axial growth rate [12]. The vapor-solid (V-S) deposition is found to increases with increasing temperature. Wires grown at lower temperatures are twelve sided, alternating {110} and {211} faces. The {110} faces are more favorable sites for V-S deposition than {211} [35]. As the temperature is increased, increased deposition on the {110} faces results in more material being added to the {110} faces in comparison to the {211} faces. As a consequence, the {110} faces disappear as the surface area of {211} facets increase, resulting in a six-sided wire with all {211} faces. Further increasing the temperature, causes three of the six {211} faces grow at the expense of the other {211} faces. At about 1300 ºC, VLS and V-S growth rates become comparable [35].

Temperature changes during growth also affect the diameter of the wire. Since the liquid surface tension is inversely related to the temperature when the temperature is reduced, the droplet contact angle changes in order to balance the increase in liquid surface tension as per Nebol'sin stability criterion [17]. Thus, the cross section of the wire decreases gradually and stabilizes when the temperature is reduced. While changing the temperatures during growth, it is preferable that the supply of silicon precursor should be reduced or stopped completely, and the temperature needs to be reduced gradually. Rapid temperature changes may cause small droplets to be pinched off from the seed droplet, leading to the formation of branches. An increase in temperature would result in an increase in the cross section. For such a gradual increase in temperature, it is useful if the proportion of silicon precursor in the carrier hydrogen gas is increased. This prevents the re-melting of silicon at the liquid-solid interface which may destabilize the <111> interface. In

extreme cases, the droplet may lose its stability and run down the side faces, causing uncontrolled growth.

2.3.2 The Role of hydrogen

Hydrogen is used as the carrier gas in the VLS process. At elevated temperatures, pure silicon and some of the silicon precursors and dopant gases are highly reactive with oxygen or water vapor. Hence, the presence of hydrogen environment prevents the oxide formation on the wires. The flow rate of hydrogen in the chamber determines the background pressure at which the growth happens. The hydrogen gas provides a reducing atmosphere in which the silicon precursor/dopant gases at the droplet surface, enabling the formation of elemental silicon/dopant species that is incorporated into the droplet. The presence of hydrogen as background gas reduced the radial growth rate either by suppressing the dissociation of silane (SiH_4) [40], [41] or by suppressing the absorption of reactants onto the silicon surface through surface passivation [42]. This would reduce the tapering along the axial direction in the wires grown. Also, hydrogen gas has been identified to reduce surface roughness of the wires by passivation in a way similar to that observed in thin films [43].

2.3.3 The Role of the Silicon Precursor

Silicon precursors like silane (SiH_4), disilane (Si_2H_6) and silicon tetrachloride ($SiCl_4$) have been used to grow silicon whiskers. These silicon precursors dissociate on the surface of the droplet and gets incorporated into the droplet. The growth rate depends on the temperature and the choice of silicon precursor. The pressure in the growth chamber is mainly dependent on the choice of gaseous silicon precursor and its cracking probability at the droplet surface [14]. Growth using Si_2H_6 can be done at extremely low partial pressures of Si_2H_6 (10^{-8} – 10^{-5} Torr) [38], whereas, the partial pressure of SiH_4 required for wire growth is five orders of magnitude higher.

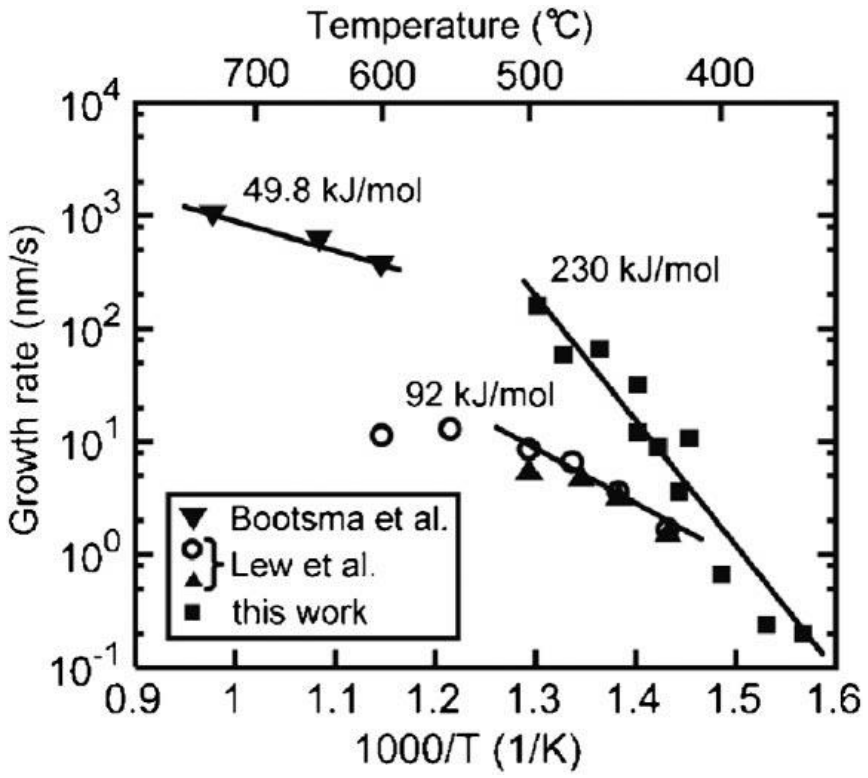

Figure 2-7 Change of growth rate with temperature for silicon nanowires for d=3-40 nm (labelled- "this work" [44]), d=100-340 nm (labelled-Lew et. al [45]), d=0.5-1.6 um (labelled-Bootsma et.al [13]) using SiH_4 as silicon precursor. Reprinted with permission from [44]. Copyright (2005) American Institute of Physics.

The growth rate of whiskers shows an Arrhenius relationship with the deposition temperature. The activation energy for the growth process can be estimated from the slope of this Arrhenius relationship. This value of activation energy can then be correlated to the rate determining step. The activation energy of the growth process for gold-catalyzed silicon whisker diameters in the range 3-40 nm is 230 kJ/mol [44], for diameters in the range 100-340 nm is 92 kJ/mol [45] and for diameters in the range 0.5-1.6 μm is 49.8 kJ/mol [13] (see Figure 2-7 [44]). The activation energy of the decomposition of SiH_4 (E_a) ranges between 213 and 234 kJ/mol in the temperature range of 375-1200 ºC [44]. The reduction of activation energies for each of the growth processes in

comparison to E_a is attributed to the catalytic decomposition of SiH_4 at the surface of liquid droplet and the rate determining step is decomposition of SiH_4 in all the three studies.

The growth rate of the silicon microwires is proportional to the partial pressure of the silicon precursor (SiH_4 [13], [44], Si_2H_6 [38], $SiCl_4$ [46]) in the growth chamber. Wagner et al. [35] estimated the growth rate V (cm/sec) for a given total gas flow rate f (cm^3/sec), a $SiCl_4/H_2$ mole ratio fraction m_R and reaction tube's cross section A (cm^2) as:

$$V = \frac{f m_R M}{\rho A V_o}$$

where M is the molecular weight of $SiCl_4$, V_o is the standard volume of a perfect gas and ρ is the density of solid silicon. The assumptions made in arriving at this equation included that the system has a high flow rate, that the condensation coefficient (i.e. the probability of a gaseous species to condense) is unity for the liquid alloy, and the absence of a disproportionation reaction that would detract from the efficiency of growth (i.e. Si not ending up as a part of the microwire). Kodambaka et al. [38] reported that the growth rate of silicon nanowires (dL/dt) is proportional to the partial pressure of Si_2H_6 and the proportionality constant is related to the reactive sticking probability S of an incident Si_2H_6 molecule. The sticking probability S is calculated using

$$S = \frac{{dL}/{dt}\, A_{wire} \rho_{Si}}{2F A_{drop}}$$

where A_{wire} is the cross-sectional area of the wire, A_{drop} (~$2A_{wire}$) is the surface area of the hemispherical droplet, ρ_{Si} is the atomic density of silicon and F is the Si_2H_6 flux which may be estimated from the measured pressure. Bootsma *et al.* [13] used an expression for growth rate *g* from the kinetic theory of perfect gases in which growth happens as a result of the number of effective collisions of vapor molecules on a surface. The growth rate for the decomposition of SiH_4

gas molecules that results in the formation of a solid phase Si (Si vapor pressure is much smaller than the pressure of impinging SiH_4 molecules) is calculated as follows:

$$g = \alpha \frac{p}{\rho} \sqrt{\frac{M}{2\pi RT}}$$

where p, T are pressure and temperature of the SiH_4, M is the ratio of the square of the molecular weight of Si to the molecular weight of SiH_4 ($M = M_{Si}^2 / M_{SiH_4}$), ρ is the density of silicon, R is the gas constant and the factor α is the efficiency of the collision process or the fraction of impinging SiH_4 molecules yielding in a free radical Si molecule. The value of α may be given by

$$\alpha = \alpha_o \exp(-E/RT_S)$$

where T_S is the temperature of the substrate and α_o is the temperature independent factor and E is the activation energy. The values of α_o and E are characteristic of the decomposition reaction.

Wagner's model [35] shows that there is an empirical relationship and this was derived based on the concentration gradient of silicon at the liquid-solid interface. Calculation of growth rate from this relation is reasonable only under growth conditions that have limited supply of silicon from the vapor. The other two models by Kodambaka [38] and Bootsma [13] are derived based on the sticking probability of the silicon precursor gas molecules on the catalyst droplet and is applicable for growth processes where the rate limiting step is determined by the Si incorporation. To apply any of these models, the activation energy may be calculated from the Arrhenius relation for a VLS growth process. This activation energy, in comparison to the activation energies of each of the steps of a VLS growth process, would help finding the rate determining step for a VLS growth process, based on which one of the above three models discussed can be chosen.

There are deviations from the ideal uniform growth rate model for VLS growth of silicon wires. Some of the non-idealities are due to the diffusion of metal catalyst from or to the droplet. At the beginning of the growth, the growth rates are slow and non-uniform (a typical seeding effect). When the metal droplet is supersaturated with Si the growth rate becomes constant. As the metal catalyst diffuses away from the droplet, the size of the droplet reduces, and the droplet maintains its composition by crystallizing the silicon at the liquid-solid interface at an increasing rate (increased growth rate). The deviation δ in the linear growth rate due to the changes in the size of the droplet is given by the relation [38]:

$$\delta = -f\frac{dV}{dt}/\pi(d/2)^2$$

where f is the volume fraction of silicon in the droplet, dV/dt is the rate of change of droplet volume and d is the diameter of the droplet. In general, wires with increasing diameters as they grow exhibit a decrease in growth rate while wires with decreasing diameters as they grow exhibit accelerated growth rates [38]. The tapering of the wire as it grows could be a result of the metal catalyst being consumed from the droplet and not just because of the sidewall deposition [38]. Consumption of the metal catalyst (incorporation into the microwire) causes the droplet to shrink as the wire grows. In turn, the cross-section of the wire (related to the diameter of the droplet) will decrease as the wire grows.

Another important parameter that determines growth rate is the diameter of the droplet. Givargizov's argument [12], [34] that the wire growth rate depends on the level of supersaturation and thus, on the wire diameter would be valid for growth near equilibrium or when the growth rate reflects a kinetic competition between silicon adsorption and crystallization. The rate of crystallization exhibits a Gibbs- Thomson effect, because the silicon chemical potential is constant,

hence the growth rate is expected to depend on the wire diameter. In Figure 2-8 the variations of growth rate are shown as functions of the wire diameter at different molar concentrations of $SiCl_4/H_2$. It can be seen that whiskers with smaller diameters grow slower than those with larger diameters [12]. There exists a critical diameter at which the growth completely stops as a result of decrease in growth rate when supersaturation decreases (growth rate is proportional to square of supersaturation). The critical diameter reduces with an increase in the molar concentration of $SiCl_4/H_2$ i.e. supersaturation [12] i.e. higher pressures are required to grow whiskers of smaller diameters [47]. There are reports confirming such a diameter dependence and the existence of a critical diameter [44].

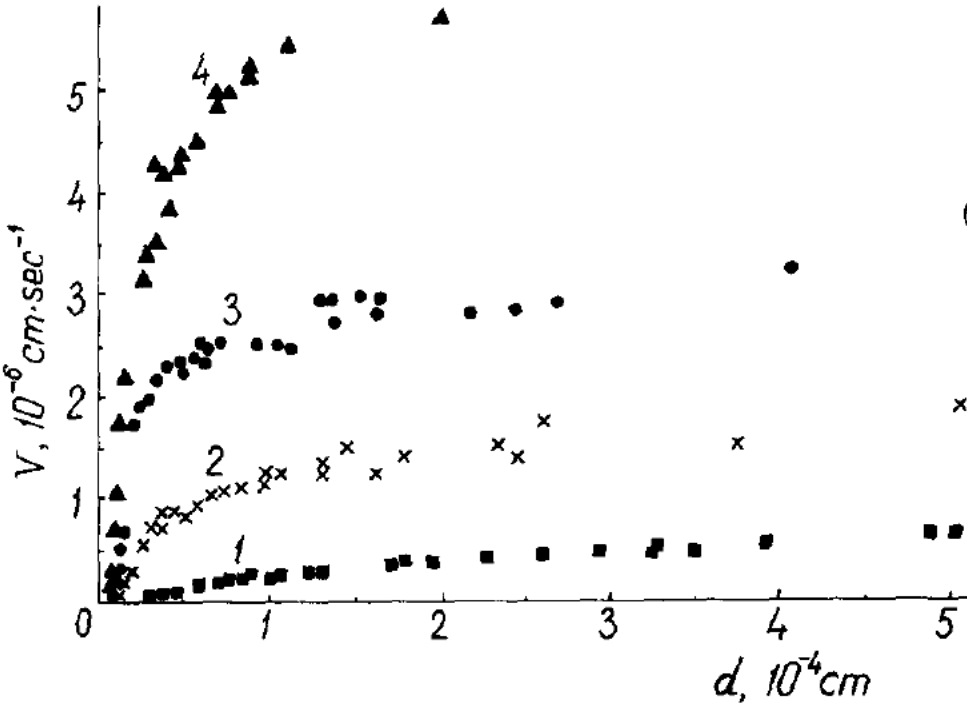

Figure 2-8 Variation of measured growth rates of silicon whiskers with diameter for various molar concentrations $SiCl_4/H_2$ i.e. supersaturations (levels of supersaturations increasing from1 to 4). Reprinted with permission from [12]. Copyright (1975) North-Holland Publishing Company.

However, there have been reports that are not in agreement with Givargizov's explanations [38], [48] because of differences in growth mechanisms or silicon precursor used. Schubert *et al.* found that the growth rate of molecular beam epitaxially (MBE) grown silicon nanowires increases with decreasing diameter. This contrary behavior is attributed to the strong surface diffusion of silicon in whisker growth by MBE which results in a larger growth rate when diameter is reduced [48]. Kodambaka et al. reported that the growth rate of nanowires grown using disilane (Si_2H_6) as silicon precursor was found to be independent of diameter [38] as shown in Figure 2-9. It was suggested that the rate determining step for whisker growth under these conditions is due to the thermally activated metal catalyzed dissociative adsorption of Si_2H_6 on the catalyst droplet [13], [38]. This is confirmed from the linear dependence of growth rate with partial pressure of silicon precursor which implies a constant sticking probability (S) despite the varying chemical potential. It was suggested that these conclusions do not depend on the low pressures used in the study or on any particular property of Si_2H_6, but are applicable to any system where growth occurs by a thermally activated metal catalyzed dissociative adsorption process occurring on the catalyst droplet [38].

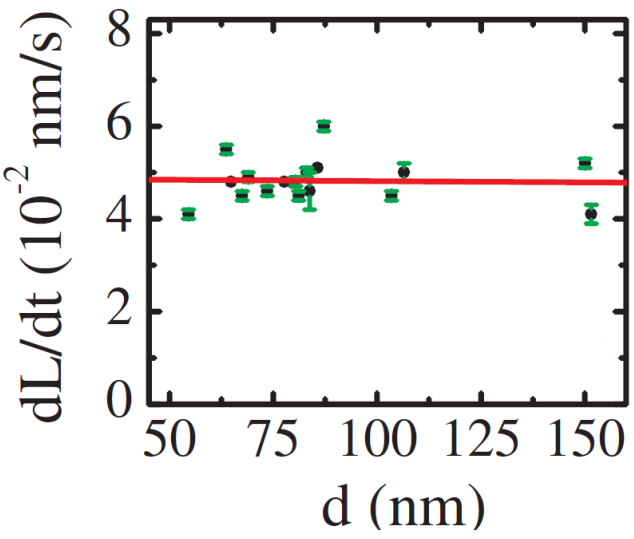

Figure 2-9 The dependence of growth rate (dL/dt) with diameter (d). The solid line represents the least square fit. Reprinted with permission from [38]. Copyright (2006) American Physical Society.

2.3.4 Doping

The electronic properties of a semiconductor material may be varied by adding impurity atoms to the pure semiconductor. The position of the impurity level in the silicon band gap is a function of the type of majority carriers (electrons or holes). The concentration of the majority carriers depends on the number of impurity atoms substitutionally incorporated into the silicon crystal lattice. Conventional methods of doping, such as ion implantation and diffusion, are used to dope bulk semiconductor materials. However, due to the high aspect ratio of the silicon whiskers, it difficult to use such methods for doping microwires. A more practical approach involves using *in situ* doping during the VLS growth. Flowing p-type or n-type dopant gases along with the silicon precursor into the growth chamber the microwires may be doped *in situ*.

The dopant atoms are incorporated into the whiskers while it is growing either through radial deposition or through the metal droplet. Wallentin *et al.* [49] explained the dopant incorporation processes using a theoretical model illustrated in Figure 2-10. The model examines the competing processes involved in dopant incorporation, namely, the dopant flux from the vapor to the liquid, J^{LV}, the dopant flux from liquid to solid, J^{LV} and the re-evaporation from liquid to vapor, J^{EV}. The segregation co-efficient (C_S/C_L - where C_S and C_L are the solubilities of dopant atoms in solid and liquids phases respectively) at the liquid-solid interface. This ratio determines the rate at which dopants atoms are incorporated into the whiskers.

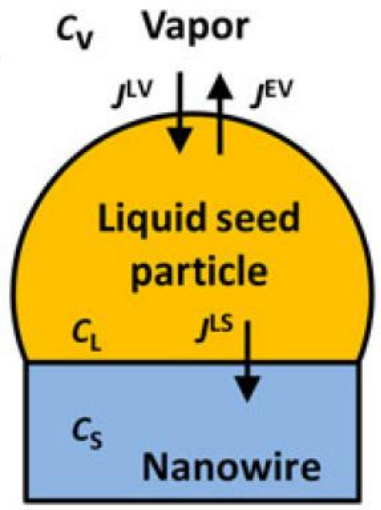

Figure 2-10 Schematic of axial dopant incorporation showing various dopant fluxes and concentrations. Reprinted with permission from [49]. Copyright (2011) Materials Research Society.

Based on dopant solubility in the metal droplet, C_S, the dopants are divided into two categories defined as being type A or type B. Type A dopants have a low solubility in the droplet and high segregation coefficient, thus making the flux from vapor to liquid, J^{LV}, the rate determining step for axial incorporation of dopant atoms. Phosphorus doping using phosphine (PH_3) in silicon nanowires is an example of a type A dopant. Schmid *et al.* [50] found that the phosphorus doping concentration was increased with the increasing molar concentration of phosphine until the solid solubility limit of phosphorus in silicon was reached. Type B dopants have high solubility in the droplet and low segregation coefficient, thus the dopant concentration is mostly determined by the segregation coefficient and not the dopant gas molar concentration. Low solubility or high segregation coefficient limits the memory effect (presence of residual impurity atoms in the catalyst droplet after that dopant gas flow was stopped) of the dopant atoms and enables the growth of abrupt heterostructures.

The dopant atoms may be incorporated in the radial growth via adsorption and capture [49]. Dopants with high solid diffusivity may diffuse into the whiskers through the sidewall facets. The dopant atoms could diffuse out through the sidewall facets when the dopant source is turned off (effectiveness of such a process is not observed experimentally). The presence of dopant atoms in the growth chamber effects the growth rates and sidewall faceting of the whiskers.

Givargizov et al. [51] observed periodic instability and changes in faceting during the growth of undoped silicon and germanium whiskers with high temperatures and high molar concentrations of $SiCl_4$ which was attributed it to the surface energy effects. The addition of $AsCl_3$ to the gaseous reaction mixture prevented these instabilities, even at most appropriate conditions for instabilities to develop. It was determined that $AsCl_3$ improved the wetting of the seed particle. Using diborane as the dopant precursor resulted in saw-tooth faceting on the sidewalls of silicon nanowires which was not observed in cases of undoped and PH_3 doped segments [52]. However, when a growth sequence of undoped segment followed by diborane doped segments was used, faceting was observed on the undoped segments in nanowires. This observation led to the conclusion that faceting was due to the radial overgrowth,

The addition of dopant precursors to the reaction mixtures affects the radial and axial growth rates of the silicon whiskers [49]. The doping of silicon nanowires with diborane created an amorphous silicon shell [53] which could be made crystalline by annealing it at high temperatures. Diborane improves the decomposition of silane and thus boosting the radial deposition. When diborane was replaced with trimethylboron, no amorphous shell was observed in case of trimethylboron because of its higher stability [54]. Unlike diborane, the n-type dopant precursor PH_3 does not have strong effects on growth of silicon whiskers [55]. Phosphine (PH_3) has minimal effect on growth rate and does not induce tapering by sidewall deposition [50]. Hence PH_3 is a better choice for n-type

doping. Schmid *et al.* [50], however, also observed that when PH_3:SiH_4 ratios higher than 2×10^{-2} are used, nanowire nucleation (growth) seems to be inhibited. This behavior is similar to the case where arsine [50] is used as an n-type dopant, which is known to affect the growth of silicon whiskers by changing the surface tension balance [12], [54].

The resistivity of n-type doped silicon whiskers grown using PH_3 as the dopant precursor, is inversely proportional to the PH_3:SiH_4 volume ratios [14]. The annealing of such silicon whiskers did not reduce the resistivity, suggesting that for *in situ* doping through PH_3, most of the incorporated donors are substitutional and therefore electrically active [50]. On the contrary, the resistivity of p-type doped silicon whiskers grown using diborane as the dopant precursor is not as consistent as the PH_3 doped wires. One reason for such an inconsistency in the resistivity values could be because of the growth of an amorphous shell when diborane is used as a dopant precursor. The amorphous silicon has higher resistivity values compared to crystalline silicon for a given dopant concentrations (This was discovered by Spears *et al.*[56] when developing amorphous Si, they found they needed large hydrogen concentrations to decrease resistivity). Trimethylboron could be used instead of diborane to avoid the growth of amorphous shell but secondary ion mass spectroscopy (SIMS) measurements over these wires showed that the boron incorporation efficiencies for trimethylboron is two orders smaller than diborane [57]. Thus, at same dopant gas pressures of trimethylboron and diborane, the resistivity values of nanowires are much higher in case of trimethylboron than diborane.

2.4 Doping by metal catalyst

Metal atoms also get incorporated as dopants into the silicon lattice during wire growth. Metals that create impurity levels close to the valence band and conduction band act as a p-type dopant (example: indium, gallium, aluminum) and n-type dopant (example: bismuth, lithium, antimony,

tellurium) respectively. The choice of metal catalyst could be made based on whether doping is intended or not in the whiskers grown.

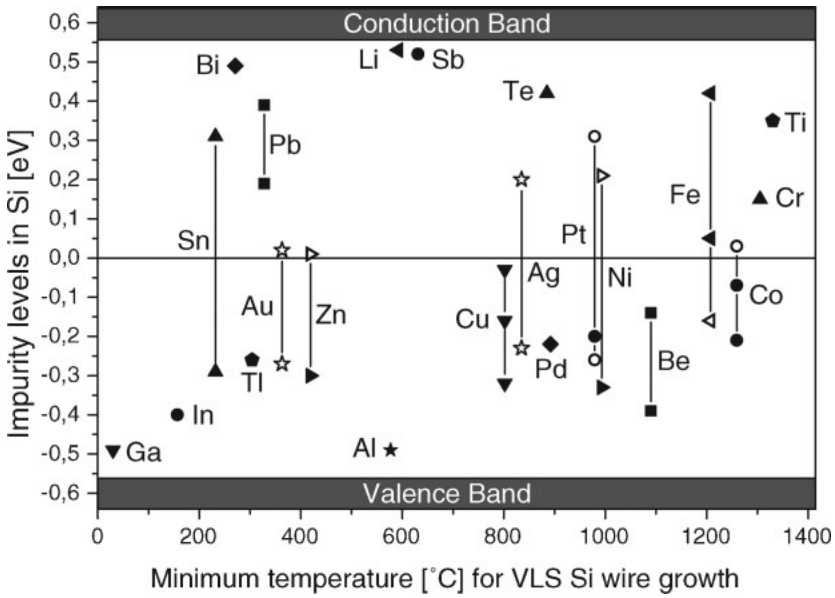

Figure 2-11 Position of impurity levels created by catalyst metals with respect to middle of bandgap. The impurity levels above mid-gap level marked with solid symbols are donor levels and open symbols are acceptor levels. The impurity levels below mid-gap level marked with solid symbols are acceptor levels and open symbols are donor levels. Reprinted with permission from [14]. Copyright (2009) Wiley-VCH Verlag GmbH & Co. KGaA, Weinheim.

Impurity levels, close to the middle of the bandgap can produce recombination centers that may determine the recombination rates and carrier lifetimes, which as stated previously are important parameters determining the efficiency of a solar device. The closer the impurity level is to middle of the bandgap the more efficient it is as a recombination center (example: gold, zinc, iron, copper, lead, cobalt). There is a threshold concentration for each dopant atoms after which the solar cell performance starts to degrade, as shown in Figure 2-12 [58]. In case of gold, the threshold doping for degradation of a solar cell performance is orders of magnitude less than other alternative catalysts.

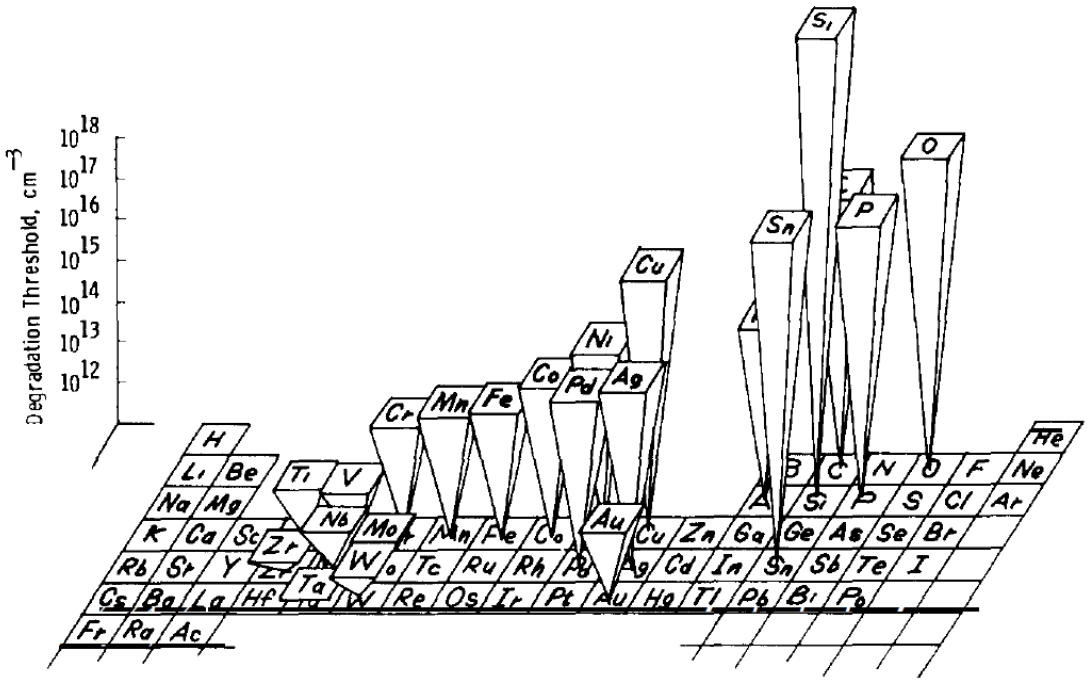

Figure 2-12 Threshold concentration of impurities for solar cell performance reduction. Reprinted with permission from [58]. Copyright (1986) Elsevier B. V.

Hall *et al.* [59] did solubility measurements on p-type and n-type silicon and observed that substantially all of the solubility in intrinsic silicon is due to interstitial copper. In the case of gold as a catalyst, it is due to substitutional impurities [60] which act as a single donor and may precipitate rapidly. In p-type silicon, most of the solubility is due to interstitial copper which is a single donor. As the p-type doping concentration increases, the solubility of copper also increases. In n-type silicon, the solubility of copper decreases with free electron concentration till the solubility reaches a minima. In this region, the solubility is mainly due to the singly charged interstitial Cu. Beyond this minima, the solubility of Cu increases approximately as the cube of the free electron concentration ($N_D > 10^{18}$ cm^{-3}), which is expected in case of a triply charged, substitutional, acceptor Cu impurity.

3 Experimental Methods

In order to fabricate silicon p-i-n microwire arrays using the VLS method, the silicon substrates are patterned with the copper catalyst to be placed in the CVD furnace. The physical and electrical properties of the microwires grown were studied in detail. In this chapter, the substrate preparation for VLS growth and electrical characterization methods used to characterize an isolated microwire will be described.

3.1 Substrate preparation

A summary of the substrate preparation process is shown in Figure 3-2. The silicon substrates used for VLS growth of microwires were fabricated using 3-inch diameter, p-type doped silicon (111) wafer (Addison Engineering, $\rho < 0.005$ Ω-cm). The substrate was cleaned in a two-step process to remove native oxide layer on the wafer. First, the wafers were RCA cleaned (piranha solution, H_2SO_4:H_2O_2 = 4:1) for 5 minutes. Secondly, the wafers were etched for 3 minutes in 1% HF solution followed by a 1 minute etch in 1% HCl. A 500 nm thermal oxide film was grown using wet oxidation (by flowing water vapor) in a furnace (Lindberg/Blue-M quartz tube furnace) at 1000 ºC for 70 minutes. The average thickness of the oxide was measured using Nanometrics Nanospec 210, at five different points on the wafer, to ensure uniform oxide thickness and was found to be 500 ± 20 nm.

The wafers were then transferred to the lithography room for patterning the oxide. Hexamethyldisilazane (HMDS) coating serves as an adhesion promoter for the photoresist. Vapor priming of the wafer using HMDS was performed using a YES-5 Oven, through a pre-programmed cycle in which the oven pumps down to dehydrate the samples and then fills pure HMDS vapor to coat the wafers. Spin coating of the photoresist (HPR 504) was completed by spreading for 10

seconds at 500 rpm and then spinning for 40 seconds at 3000 rpm. This resulted in a photoresist of uniform thickness 1.5 ± 0.2 μm, across the wafer. The wafers were then soft baked at 110 ºC for 90 seconds. After the soft bake, the wafers were left to rehydrate for about 15 minutes as it is important to ensure the proper exposure and developing of the resist.

The wafers were then exposed to UV light for 5 seconds using a chrome mask with 3 μm diameter circles, 7 μm pitch. The ultraviolet wavelengths available were 436 nm and 365 nm which are g-line and i-line of mercury. In contact printing, the finite mask to wafer separation (z) causes diffraction spreading that limits the minimum possible resolution (W_{min}) which is given by

$$W_{min} \approx \sqrt{k_C \lambda z}$$

where λ is the exposure wavelength and approximately k_c ~1.6 [61]. A wavelength of about 400 nm would lead to a minimum resolution of 3 μm, where the gap between the mask and the wafer was about 14 μm. The precise minimum achievable resolution is influenced by ambient humidity, ambient temperature and the presence of mask imperfections. The most effective control for these, to ensure consistency, is to ensure near-perfect contact between the mask and wafer to transfer the pattern.

The exposed wafers were developed using developer 354 for 20 seconds and then rinsed with DI water. The wafers were baked in an Isotemp oven at 120 ºC for 20 minutes. The wafer was observed under a microscope (Olympus BX51) to confirm an effective exposure. A successful exposure resulted in a uniform array as shown in Figure 3-1, where the dark regions represent the exposed areas (removed when developed) and bright regions represent unexposed photoresist. The wafers were then transferred to the wet bench for further processing.

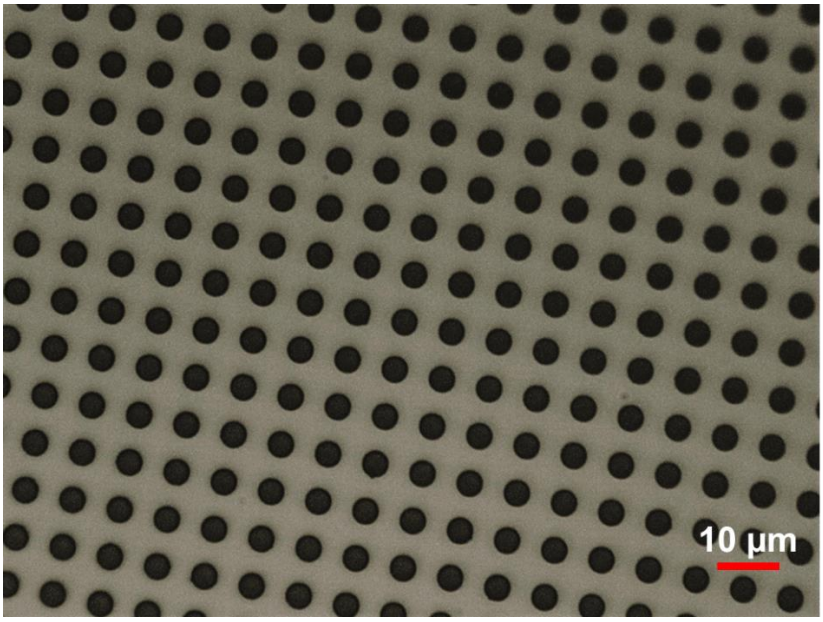

Figure 3-1 Optical image of wafer substrate post UV exposure development. The dark regions represent exposed regions and the bright regions is the photoresist.

The oxide in the regions without the photoresist was removed using 10:1 BOE (~ 10 minutes). The thermal oxide thickness was the same on both sides of the wafer. Thus, the back (unmasked) surface of the wafer turning hydrophobic confirmed the completion of the etch process. A pure silicon surface is hydrophobic. Silicon dioxide (SiO_2) makes the surface hydrophilic. After etching away the oxide, copper was deposited onto the wafer in a thermal evaporator. The thickness of the copper deposited was chosen to be about the same thickness as the oxide layer which was confirmed using AFM measurements. Following the Cu deposition, the photoresist was "liftoff"ed by washing it with acetone followed by a DI water rinse. The wafer finally had an oxide layer with holes etched in it and copper deposited inside the holes. It was critical to ensure all the oxide layer is removed. The presence of an oxide layer prevents the diffusion of copper into the silicon. The silicon and copper must form a eutectic mixture when it is heated to create microwire growth. A 10% over-etch was used to ensure removal of oxide across the wafer. It is also necessary that the

copper thickness inside the hole is less than or equal to the oxide thickness to be able to grow a uniform array of silicon microwires.

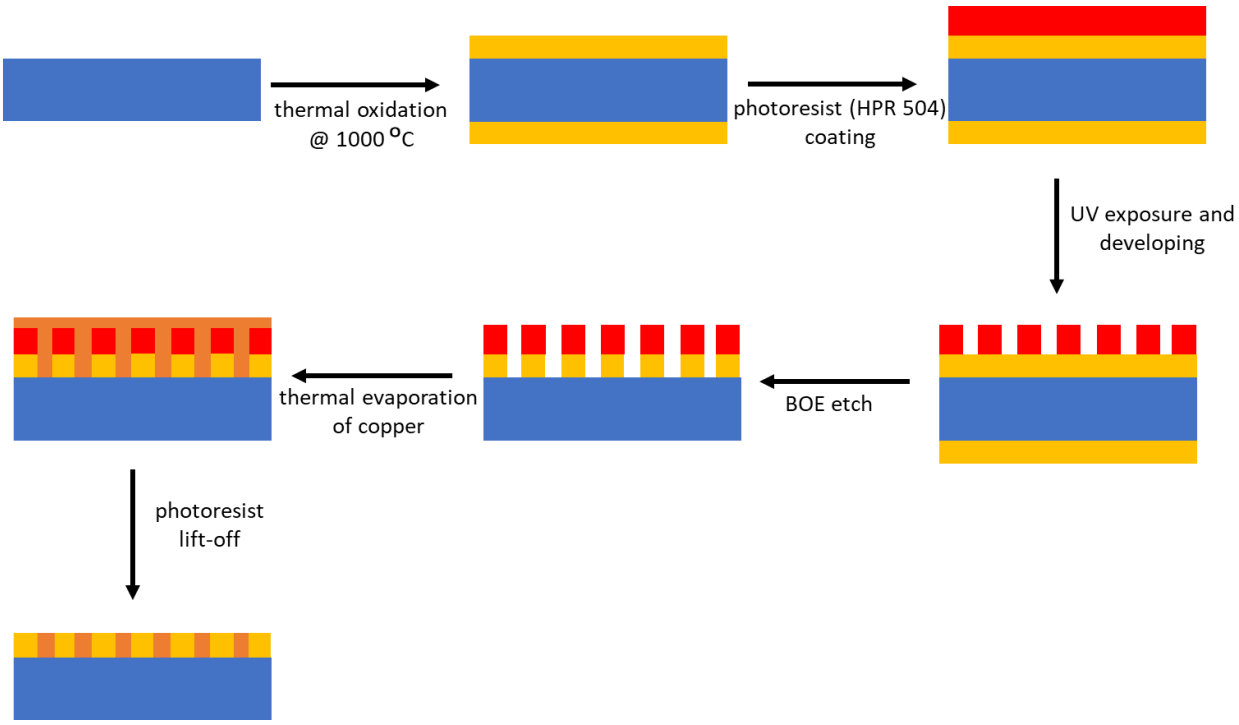

Figure 3-2 Schematic of the wafer processing used to pattern the wafers with the copper catalyst. The color representation is as follows: blue- silicon wafer, yellow- SiO_2, red- photoresist (HPR 504), orange- copper.

3.2 Growth in a CVD furnace

Silicon microwires were grown in a custom built chemical vapor deposition (CVD) reactor as shown in Figure 3-3. The wafer was cut into small pieces to produce a substrate (1 x 1 cm) that could be loaded into the reaction chamber (quartz tube) of the furnace. The growth substrates were placed 6-10 cm away from the center of the furnace, closer to the entry point of the precursor gases. A description of the furnace temperature calibration is given in Appendix A. The reaction chamber was sealed on both sides and then pumped down using roughing pump to 5 Torr. It was then filled with argon gas until the pressure reached 760 Torr. The chamber was then pumped

down again using roughing pump to ~3 Torr. The chamber was then opened to the drag pump and held at a pressure of ~0.01 Torr for 1 hour prior to microwire growth. These steps ensured that most of the oxygen and water vapor was removed. Water vapor and oxygen react vigorously with the silicon precursor gases at elevated temperatures forming silicon dioxide and a range of intermediate chlorosiloxanes [62]. Some of these reactions are shown below in Equations 3-a, b.

$$SiCl_{4(g)} + O_{2(g)} \rightarrow SiO_{2(s)} + 2\ Cl_{2(g)}$$

$$SiCl_{4(g)} + 2\ H_2O_{(g)} \rightarrow SiO_{2(s)} + 4\ HCl_{(g)}$$

The reaction chamber was heated to 1000 ºC under $H_{2(g)}$ (6.0 Semiconductor Process Grade, Praxair Inc.). A separate line of H_2 is used to draw silicon tetrachloride ($SiCl_4$) vapor from the source tank (liquid $SiCl_4$, fiber optic grade 99.9999%; Strem Chemicals) into the reaction chamber. The rate at which hydrogen flows into the $SiCl_4$ tank is used as the $SiCl_4$ flow rate in the following discussions. The hydrogen gas flowing into and through the $SiCl_4$ tank sweeps the $SiCl_4$ vapor present over the $SiCl_4$ liquid along the direction of flow. A calculation of the amount of $SiCl_4$ present in the hydrogen flowing out of the $SiCl_4$ tank is given in Appendix B. To obtain microwires of p-type doping, boron trichloride gas (250 ppm BCl_3 in hydrogen; Matheson Tri-Gas) was used as a source of boron, whereas for n-type doping, phosphine gas (100 ppm PH_3 in hydrogen; Matheson Tri-Gas) was used as a source of phosphorus. Microwires of different dopant concentrations were grown by varying the flow rate ratios of the dopant precursor and $SiCl_4$ while using the hydrogen carrier gas to ensure a consistent total flow rate of hydrogen and $SiCl_4$.

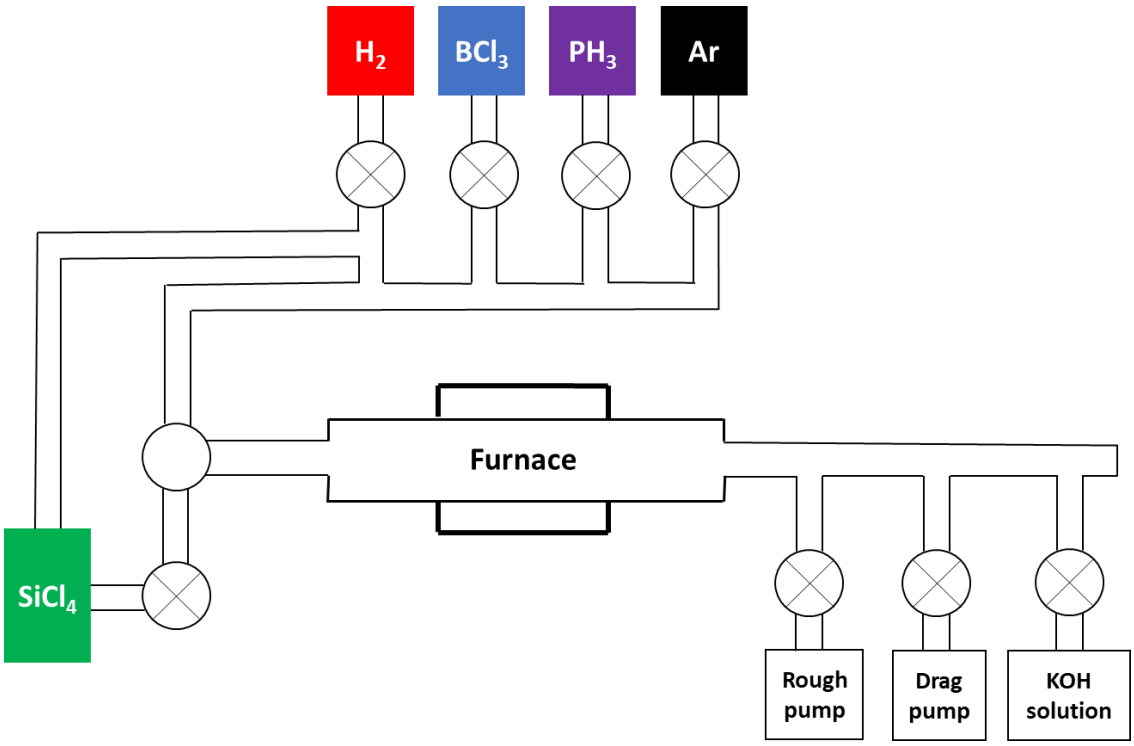

Figure 3-3 Schematic of chemical vapor deposition furnace used to grow silicon microwires.

The copper-silicon system has a eutectic temperature of ~802 ºC [20]. When the substrates are heated to 1000 ºC, a droplet of a copper-silicon eutectic mixture is formed. Microwires of different doping densities were grown by 1) changing the flow rate of $SiCl_4$, while keeping the total flow rate of hydrogen and $SiCl_4$ at 500 sccm (standard cubic centimeters per minute) or 2) changing the flow rate of dopant gases (BCl_3, PH_3). The silicon precursor ($SiCl_4$) and dopant gases react at the droplet surface where the elemental silicon and the dopant atoms are incorporated into the droplet according to the following reactions:

$$SiCl_{4(g)} + 2\,H_{2(g)} \rightarrow Si_{(g)} + 4\,HCl_{(g)}$$

$$2\,BCl_{3(g)} + 3\,H_{2(g)} \rightarrow 2\,B_{(g)} + 6\,HCl_{(g)}$$

$$2\,PH_{3(g)} \rightarrow 2\,P_{(g)} + 3\,H_{2(g)}$$

The unreacted precursor gases and any remaining reaction products leave the reaction chamber, entering a 6M KOH bath in which they were oxidized. The KOH bath was kept open to atmosphere throughout the duration of the wire growth, thus maintaining the chamber pressure at 760 Torr (atmospheric pressure) during the reaction. Phenolphthalein, a commonly used indicator in acid-base titrations was used in the KOH bath to indicate when the solution required replacement. The threshold for this would be the solution becoming neutral (at pH~8). The growth times of the wires were chosen such that the lengths of the wires (~120 µm) grown were enough to allow for electrical measurements.

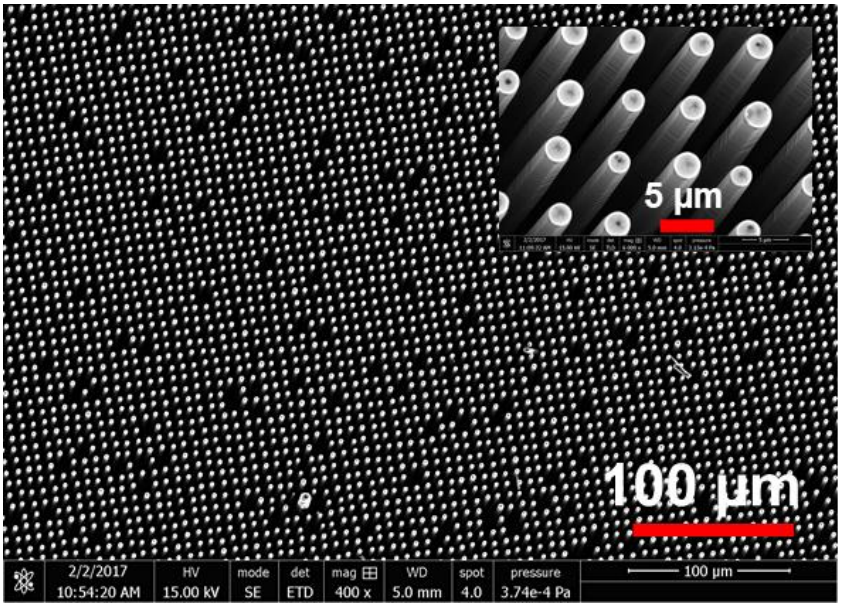

Figure 3-4 Scanning electron microscope (SEM) image of the microwire arrays grown using the VLS technique in this study. Inset shows an identical array of microwires with metal catalyst at the tip of the microwires.

3.2.1 Silicon Microwire Growth at 950 ºC

The influence of sidewall deposition on the choice of flow rates used for growth could be minimized by reducing the growth temperature [35]. Wires were grown at 950 ºC by first flowing

$SiCl_4$ (10 sccm) at 1000 ºC for 5 minutes to saturate the droplet with silicon. The temperature was then lowered to 950 ºC and the flow rate of $SiCl_4$ was reduced to 1 sccm [35]. The temperature was dropped from 1000 to 950 ºC in two different techniques. In the first of these techniques the temperature is reduced at 1 ºC/min. In the second technique, the set point is just lowered to 950 ºC and the furnace is allowed to cool for ~ 5 minutes. With either technique, when the temperature is stable at 950 ºC the flow rate of $SiCl_4$ was then increased back to 10 sccm and grown for 20 minutes.

3.3 Electrical measurements

The microwires were separated from the substrate using a razor blade by scraping a corner of the substrate which was suspended in acetonitrile (HPLC grade, Sigma Aldrich). The suspended microwires tend to aggregate and thus the suspension was sonicated for 4-5 minutes. The microwires were then transferred onto a glass slide using a 10 µL micropipette. The resistivity and doping concentrations of the microwires were calculated from four-point probe measurements on individual microwires. The individual probes were controlled by piezoelectrically driven units (Imina Technologies micromanipulator miBot BT-11).

The most common way used to form ohmic contact to semiconductor micro/nano-structures is to thermally evaporate metal contacts onto the wires. For the diameters of microwires (> 1.5 µm) in this study, the metal films required to ensure reliable ohmic contact are too thick for a lift-off process [63]. However, it has been shown that direct and reliable ohmic contacts to silicon microwires could be established using tungsten probes by applying sufficient local mechanical pressure [64]. The resistivity and band structure of silicon was reported to vary as a function of applied pressure [65], [66]. Applying a pressure of ~ 11 mN μm^{-2} on planar silicon, it was reported that a local phase transition from Si-I (semiconductor) to Si-II (metallic) [67], [68] can occur. Such

a direct contact formation technique avoids the extra lithography steps required for thermal evaporation of metal contacts.

For making direct contacts, tungsten probes with a tip radii 2 µm (American Probe and Technologies) were etched in 2M KOH solution for ~30 seconds to remove any tungsten oxide. Two-point electrical measurements were made using a single pair of tungsten probes to make direct contact by applying a local pressure > 11 mN μm^{-2} [64], [69] and recording the I-V response. To perform four-point measurements, electrical contact to the microwire was first established using the outer probes which are used to drive the current through the wire. The inner probes were used for voltage sensing by placing them in contact with the microwire. A current-voltage (I-V) response was recorded using an Agilent B1500A semiconductor parameter analyzer [70]. Successful, hysteresis free (around I=0) four-point measurement were obtained by using an intermediate local pressure regime (2-11 mN μm^{-2}) for the inner probes along with the local pressure regime (>11 mN μm^{-2}) for the outer probes.

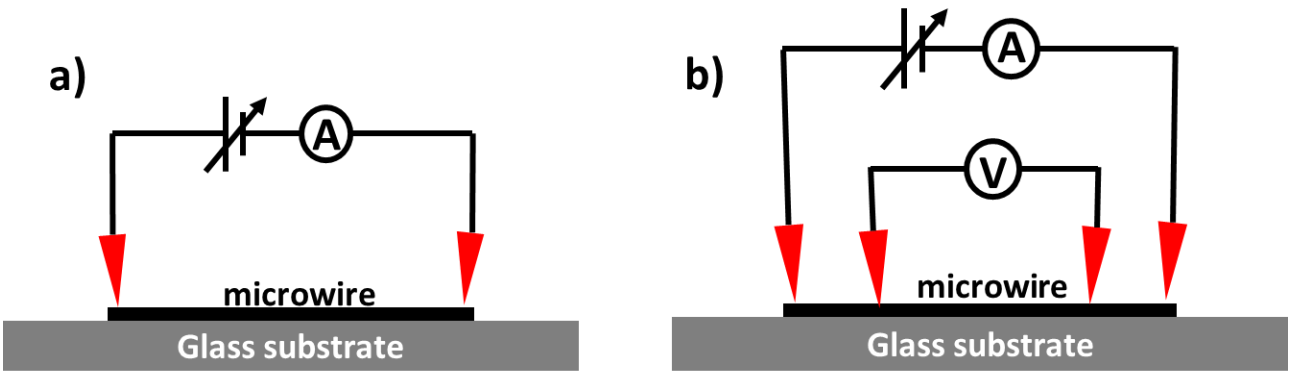

Figure 3-5 Schematic of a) two-point measurement where direct contact is made by a pair of probes to record the V-I response. b) four-point measurement showing the outer and inner probes as connected to the semiconductor device analyzer (Agilent B1500A). The outer probes were positioned to the ends of the microwire and the spacing between the inner probes was changed to have different probe separations and was used to measure the resistivities of various sections of the microwire.

4 Results and Discussion

The ability to grow microwires with desirable physical and electrical properties is the first step towards successful implementation of these structures into a water splitting cell. The properties of the microwire structures were varied by changing the flow rates of the gases and temperature. The physical properties of the resulting wires were observed using a scanning electron microscope (SEM) and the electrical properties (doping) were measured using four-point probe measurements. In this chapter the impact of growth conditions on the microwire properties are presented. This allows for the optimization of the growth conditions to produce p-i-n microwires for an efficient water splitting device.

In this study, copper was used as a metal catalyst for growth of microwires using VLS mechanism. Copper was chosen as the catalyst as opposed to gold as it is more abundant and cheaper. Copper also has higher threshold for solar cell degradation than gold [58]. Finally, the copper-silicon system has higher percentage of silicon at its eutectic temperature. From the phase diagram of the Si-Cu eutectic shown in Figure 4-1, it can be seen that the eutectic has ~ 18% Si, by weight. Also, the Si-Cu eutectic offers higher growth rates than gold [26]. The copper atoms get incorporated into the wire during growth along with the dopant atoms. To establish the nature of doping by the copper atoms, microwires were grown by flowing only the $SiCl_4$ precursor gas. The resultant microwires had measured resistivities equivalent to n-type doping on the order of 10^{17} cm^{-3}, which is on the same order as the solubility limit of copper in silicon at the growth temperature of 1000 ^{o}C, however precipitation and out diffusion of copper [71]–[73] still occurs. The n-type nature of the copper atoms was confirmed through four-point electrical measurements on an intrinsic-p composite microwire which will be discussed in detailed later in this chapter (section 4.5).

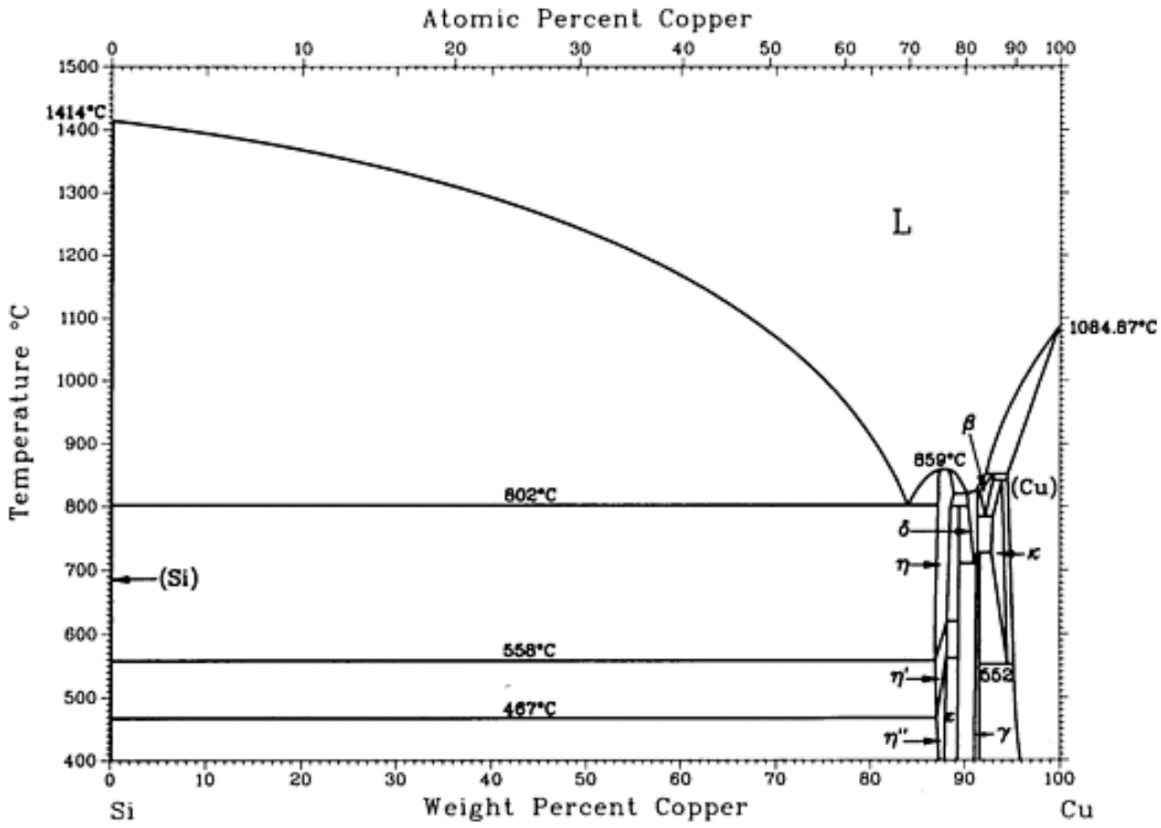

Figure 4-1 Phase diagram of a copper-silicon eutectic system [15].

The different microwires used in this study were grown by changing the flowrates of the silicon precursor ($SiCl_4$), the p-type dopant gas (BCl_3) and the n-type dopant gas (PH_3). In Table 1 the various flow rates used for the p-type and n-type samples are listed. Samples p1-p4 were grown by varying the flow rate of $SiCl_4$ as 1, 3, 5 and 10 sccm while maintaining a total flow rate of $SiCl_4$ and hydrogen at 500 sccm. The flow rate of BCl_3 was maintained at 22 sccm in all the four samples. The samples p1, p2 were grown for 15 minutes and p3, p4 were grown for 60, 360 minutes respectively, to ensure that the wires were long enough to facilitate the four-point electrical measurements.

Table 1 Growth conditions, the resultant growth rates and doping concentrations for the samples considered. The hydrogen carrier gas flow rate was used to ensure that the sum of flow rates of $SiCl_4$ and hydrogen in every growth is 500 sccm (p1-p4) or 490 sccm (all other samples).

Sample	Precursor $SiCl_4$ (sccm)	Dopant- BCl_3 or PH_3 (sccm)	Measured growth rate (μm/min)	Measured doping concentration (cm^{-3})
p1	1	22	0.17	9.2×10^{19}
p2	3	22	2.22	4.0×10^{19}
p3	5	22	3.78	6.8×10^{18}
p4	10	22	8.14	5.8×10^{18}
p5	10	15	7.36	5.5×10^{18}
p6	10	10	7.51	2.2×10^{16}
p7	10	1	7.42	1.7×10^{14}
n1	10	22	10	2.9×10^{19}
n2	10	15	8.67	2.7×10^{19}
n3	10	10	9.82	2.4×10^{19}
n4	10	5	9.17	1.5×10^{19}
n5	10	1	8.83	9.7×10^{17}
n6	10	0.1	7.01	1.1×10^{17}

The growth rates (μm/min) were calculated by dividing the average length of 50 microwires in each sample by the growth time. As expected, the microwire growth rates varied linearly with $SiCl_4$ precursor flowrate and as such is proportional to the partial pressure of $SiCl_4$ in the chamber [13], [38], [46]. The linear dependence is shown in Figure 4-2. The samples p5, p6, p7 were all grown for 15 minutes, with a variation in the BCl_3 flowrate as from 15, 10 and 1 sccm respectively.

The flowrate of $SiCl_4$ was maintained at 10 sccm and the hydrogen flowrate at 490 sccm. The samples n1-n6 were all grown for 15 minutes with the flowrate of PH_3 changing from 22 sccm to 0.1 sccm as shown in Table 1. Flowrate of $SiCl_4$ and hydrogen were maintained at 10 sccm and 490 sccm respectively.

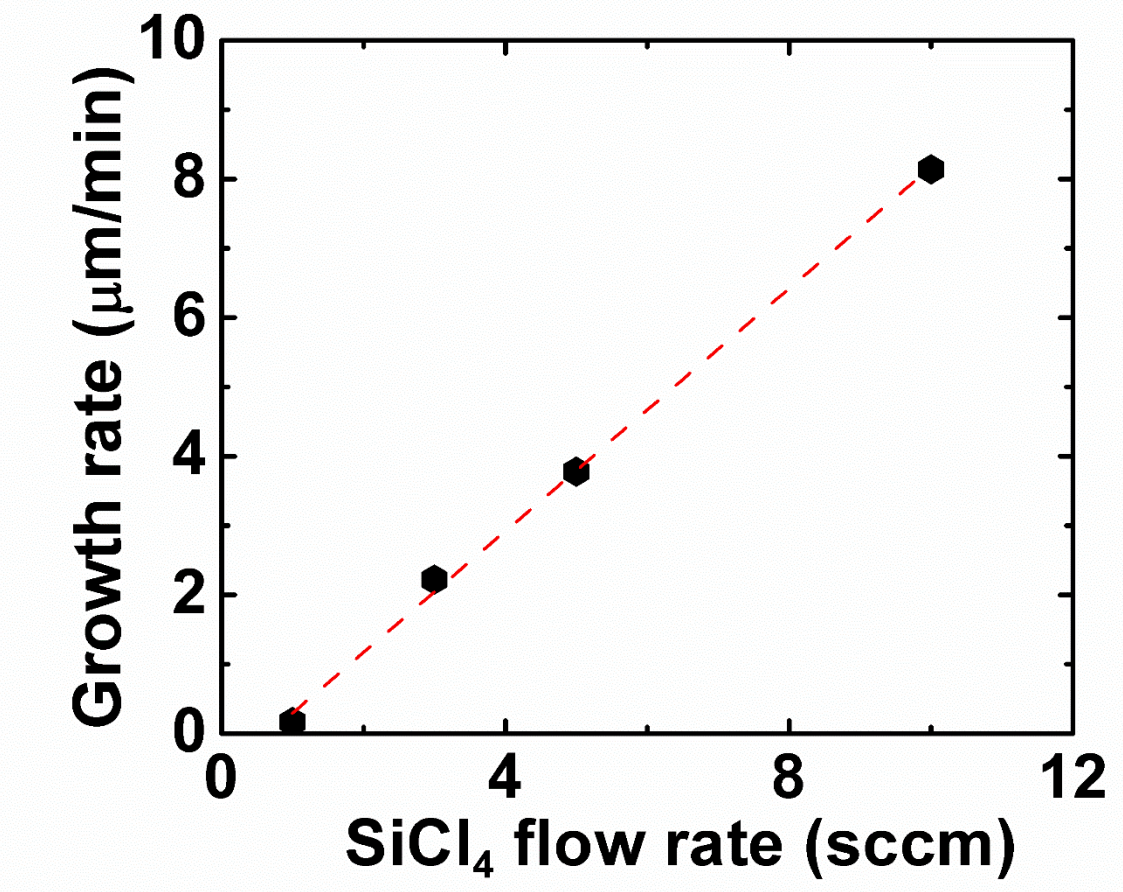

Figure 4-2 Linear response of microwire growth rate to silicon precursor flow rates (samples p1-p4). The lengths of the wires were measured on the glass slide. The measurement uncertainty is of the order of the size of the data points. The line does not pass through zero because at lower flow rates the droplet would not saturate.

4.1 Doping concentration

Independent four-point measurements were made on 30 separate microwires for each of the sample growth conditions shown in Table 1. After the direct contact was made by the outer probes, the

ohmic nature of the direct contacts was confirmed by the linear response of the measured I-V curve. The inner probes were then brought into contact with a section of the wire and the potential drop between the inner probes was recorded while current was being driven through the outer probes. The resistance of the section between the inner probes was measured from the slope of the I-V curve. It has been shown that the minimal impact of contact resistance in a four-point measurement makes it a more reliable approach [70].

Assuming a uniform flow of electric current, the resistivity (ρ) of an individual microwire can be extracted from the measured resistance (R) as

$$\rho = R\frac{A}{L}$$

where A is the cross-sectional area of the microwire and L is the length between inner probes. The doping concentration of the individual microwires is extracted from the resistivity (ρ) values using

$$\rho = \frac{1}{q(n.\mu_n + p.\mu_p)}$$

where q is the electron charge ($= 1.6 \times 10^{-19}$ C), n is the electron density in the conduction band, p is the hole density in the valence band, μ_n is the mobility of electron (≤ 1400 cm^2 V^{-1} s^{-1}) and μ_p is the mobility of hole (≤ 450 cm^2 V^{-1} s^{-1}). For a p-type semiconductor, p >> n, the equation can be simplified to $\rho = \frac{1}{qp.\mu_p}$ and for a n-type semiconductor, n >> p, the equation can be simplified to $\rho = \frac{1}{qn.\mu_n}$. The doping concentrations of both p-type and n-type samples were in the range of 10^{17} - 10^{20} cm^{-3}. However, in this regime the mobility is a strong function of doping concentration. The mobility values were estimated from previous measurements [74] to estimate the doping concentrations (final column of Table 1).

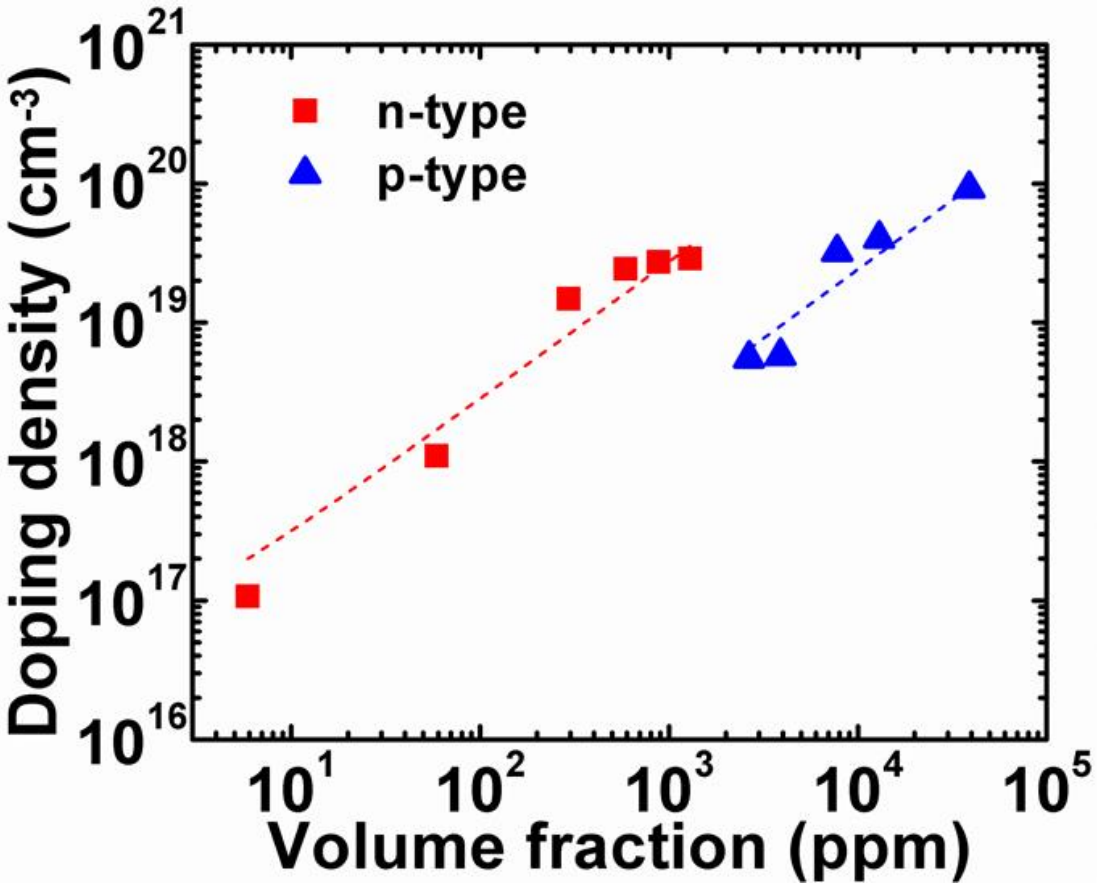

Figure 4-3 The variation of doping concentration with the ratio of dopant concentration to SiCl4 concentration in ppm for n-type doped microwires (log-log scale).

In Figure 4-3 the variation of doping concentration with volume fraction is shown for p-type (p1-p5) and n-type (n1-n6) microwires. The variation of doping concentration with volume fraction for p-type samples (p1-p7) is presented in Figure 4-4. The volume fraction of the dopant precursor gas (BCl_3 or PH_3) was calculated in parts per million relative to the $SiCl_4$ partial pressure. An example calculation of volume fraction is included in Appendix B.

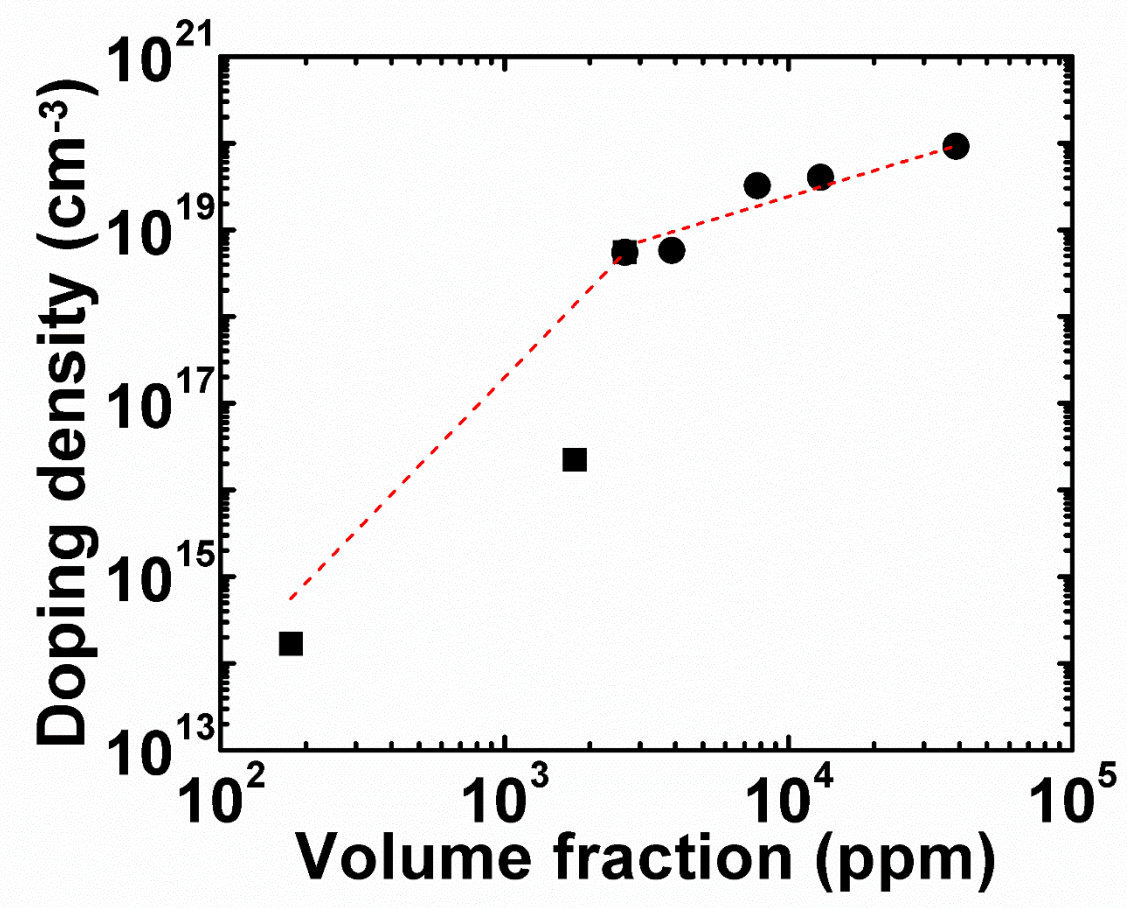

Figure 4-4 The variation of doping concentration with the ratio of dopant concentration to $SiCl_4$ concentration in ppm for p-type doped microwires (log-log scale). The data is plot as two sets based on the parameter varied during the growth process.

The lower bound of the doping concentration accessible in both p-type and n-type microwires grown using VLS technique is constrained by the presence of copper residues in the microwire. The copper incorporated acts as an n-type dopant [59] with doping densities on the order of high 10^{16} cm^{-3} which is approximately the solid solubility levels of copper in silicon at the microwire deposition temperature. This is the primary explanation for the lower doping concentration limit of 10^{17} cm^{-3} in n-type microwire growth as shown in Figure 4-3. The dopant concentration response to volume fractions of BCl_3 on the order of $10^2 – 10^3$ ppm is different from the response at higher

volume fractions as shown in Figure 4-4 reflects the extent of influence of copper residue. For volume fractions below 10^3 ppm, the extracted doping concentrations reflect a net doping concentration including contributions arising from any copper present, rather than absolute doping concentration. At higher doping concentrations, the influence of the copper residue is less pronounced. Both p-type and n-type microwires show similar variations in doping concentrations with volume fraction.

For p-type doped microwires with a doping variation of $10^{18} – 10^{20}$ cm^{-3} using copper seed, for same order of volume fraction range used in this study is smaller than gold seeded ones ($10^{12} – 10^{17}$ cm^{-3}). This could be attributed to the higher percentage of boron in the copper droplet at 1000 ºC (10-12%) [75] than in gold at the same temperature (< 0.3%) [15].

4.2 Morphologies of the microwires

The microwires grow axially in the {111} direction and have a number of sidewall facets which is a result of the sidewall deposition of silicon that happens through a vapor-solid (VS) mechanism. It has also been reported that the metal catalyst forms a layer on sidewalls of the microwire, to behave as a surface catalyst for sidewall growth [76]. The sidewalls of the microwires have dangling bonds which acts as a site for deposition of silicon atoms from the vapor phase. Surface passivation of the sidewalls of the microwires resulted in a drop in the radial growth rate [76]. The shape and size of the microwire facets depends on the surface chemistry and the exposure time of the sidewalls to VS deposition. The sidewall growth rate is two orders of magnitude less than the axial growth rate [38].

The microwire samples grown at higher flow rates of $SiCl_4$ (p3, p4) were twelve faceted with alternating {110} and {211} facets as shown in Figure 4-5a. For microwires grown at lower flow rates of $SiCl_4$ (p1 growth conditions for 120 minutes, p2) were six faceted all being {211} as shown

in Figure 4-5b. At lower flow rates of $SiCl_4$, the concentration of the reaction by-product gaseous HCl in the chamber is relatively low compared to the gaseous HCl at higher flow rates of $SiCl_4$. The presence of HCl in the chamber reduces the catalyst diffusion on the microwire surface as the Cl atoms tend to passivate the sidewall surface [76]. As a result of these factors, the sidewall growth rate increases with a decrease in the concentration of HCl in the chamber. When the radial growth rate increases, {110} facets are more prone to sidewall deposition thermodynamically than the {211} facets [35] and hence resulting in six-{211} facets.

At lower flow rates of $SiCl_4$, because of the smaller growth rates, the wires had to be grown for longer durations to have microwires having length suitable for making four-point measurements. The sidewalls in such samples are exposed to sidewall deposition for longer durations and thus more sidewall deposition occurs. When the microwires were grown for extremely long times (for example 360 minutes for sample p1), the wires almost looked triangular as shown in Figure 4-6. The large {211} facets are flat and do not show secondary faceting, indicating it is stable against silicon deposition radially [76].

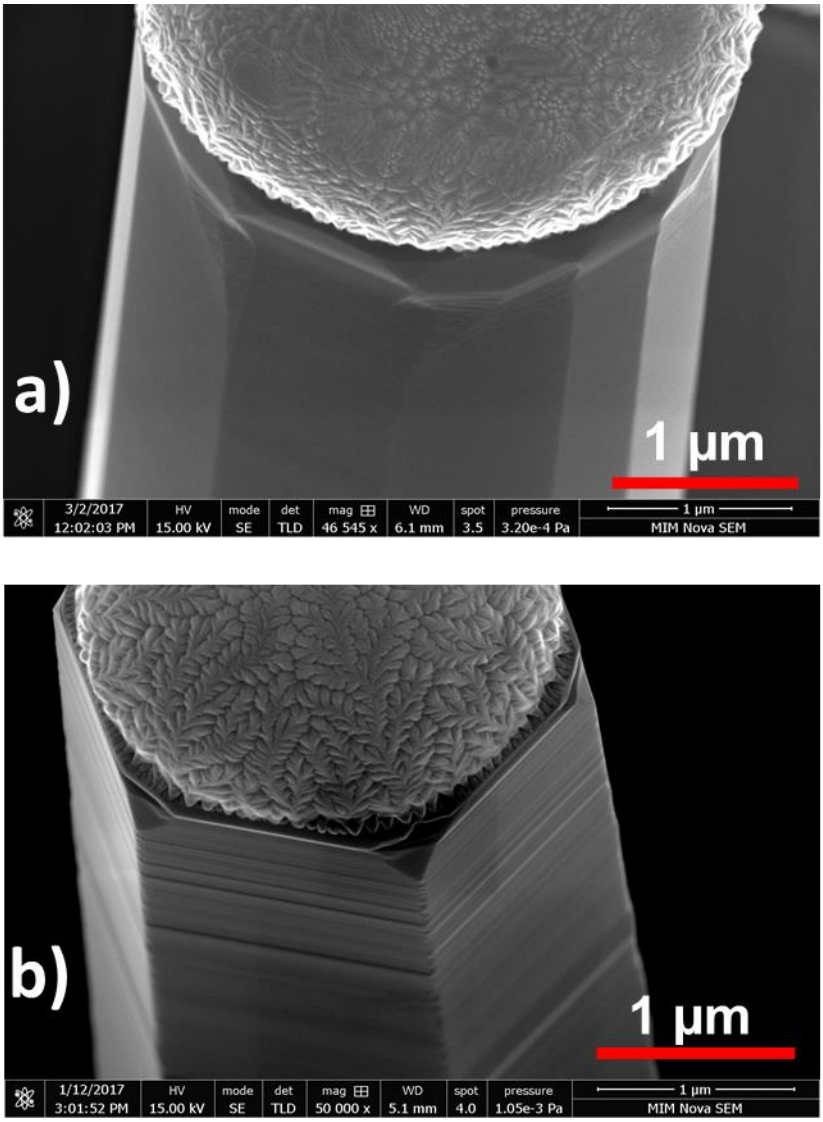

Figure 4-5 SEM images of silicon microwires a) p-type doped microwires grown in 10 sccm flow rate of $SiCl_4$ (p4) having 12 facets (alternating {110} and {211} crystal directions); b) p-type with 6- {211} facets grown in 1 sccm flowrate of $SiCl_4$ (same conditions as p1) for 120 minutes.

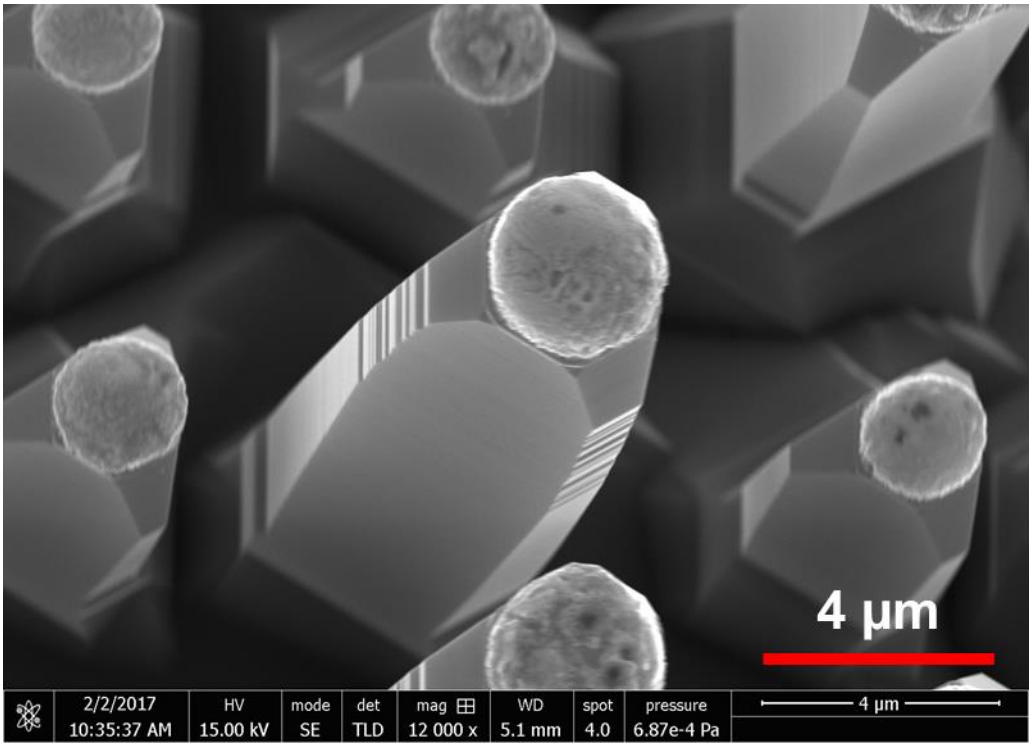

Figure 4-6 SEM image of microwire grown at 1 sccm for 360 minutes (p1). The wires look almost triangular with three of the larger facets looking flat and having no secondary faceting.

Boron, being an acceptor atom, has a strong tendency to form covalent bond with surrounding silicon atoms. The boron atoms on the surface of the microwire results in an enhanced surface adsorption of silicon atoms onto the sidewall [77]. Thus, the radial growth rate increases with boron concentration although at high concentrations of boron, the growth rate is suppressed due the precipitation of boron at the grain boundary [78]. When the flow rate of $SiCl_4$ is reduced, the increase is small in proportion to boron atoms concentration in the reaction chamber also contributes to increased sidewall deposition. The sample p4, grown at 22 sccm BCl_3 flow rate is 12-faceted and reducing the flow rate of BCl_3 from 22 sccm to 1 sccm (p4-p7) also resulted in 12-faceted wires, which is expected. The lower boron concentration in the chamber results in a

reduced sidewall deposition rate and thus the 12 facet morphology of the microwire at 22 sccm is observed at 1 sccm.

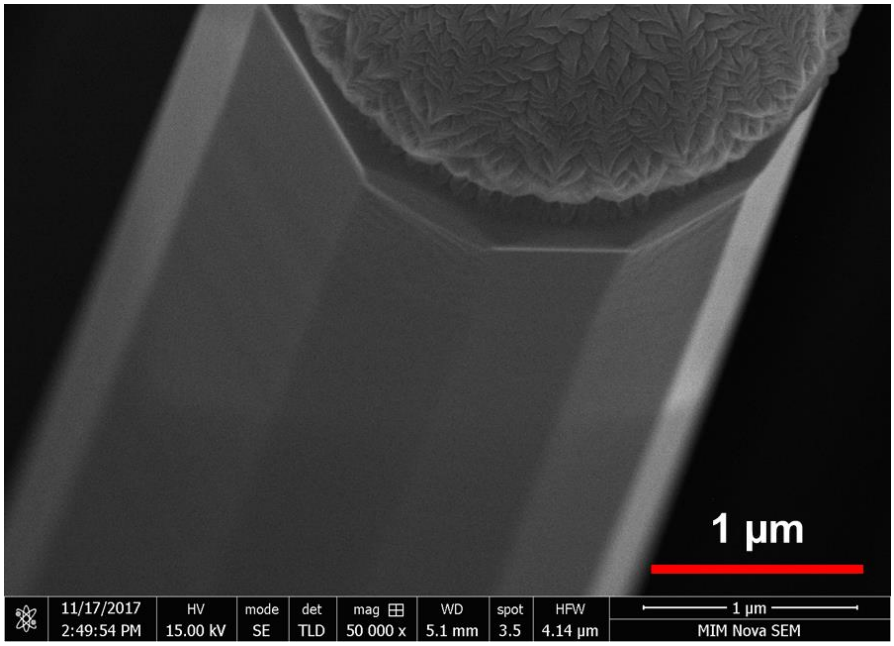

Figure 4-7 SEM image of a microwire grown at 1 sccm of BCl_3 flow rate (p7). Reduction in the concentration of boron in the reaction chamber did not alter the number of sidewalls and resulted in 12 faceted for all samples even with a change of BCl_3 flow rate (p4-p7).

Phosphorus atoms bind with the hydrogen on the sidewall surface and block the available sites for adsorption of silicon onto the sidewalls [79], [80]. Therefore, a higher concentration of PH_3 reduces the radial growth rate of the microwires. The n-type doped microwire samples n1-n6, the flow rate of PH_3 was reduced from 22 sccm to 0.1 sccm. It was observed that at higher flow rates of PH_3 (n1, n2, n3, n4), the microwires were 12 faceted, as shown in Figure 4-8a. However, the microwires grown at lower flow rates of PH_3 (n5, n6), were 6-faceted, as shown in Figure 4-8b. At lower flow rates of PH_3, the lower concentrations of phosphorus resulted in a higher sidewall deposition. When the sidewall deposition rate increases, {110} are more prone to sidewall deposition, resulting in microwires with 6 {211} facets.

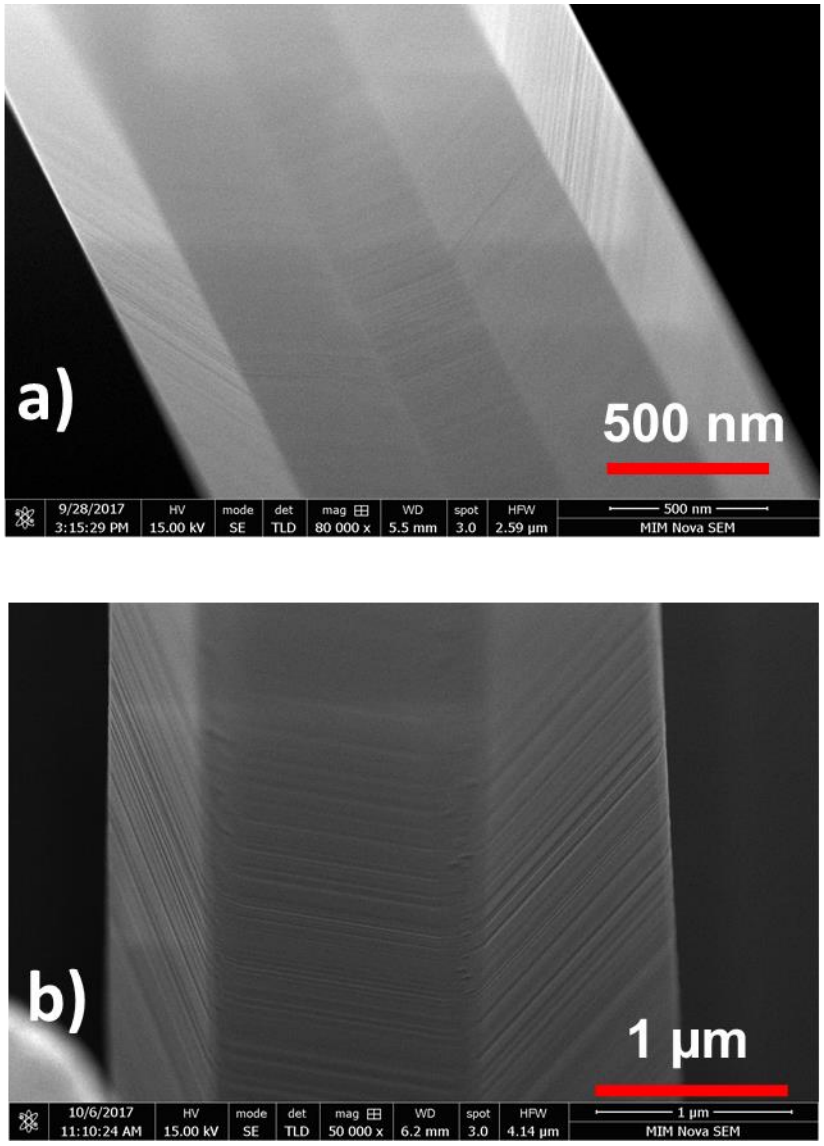

Figure 4-8 SEM image of microwires a) n-type with 12 facets (alternating {110} and {211} crystal directions) grown with 22 sccm PH3 (n1); and b) 6- {211} facets grown when PH3 flow rate was 1 sccm (n5).

4.3 Composite microwire

Composite microwires were grown by changing the flow rates of $SiCl_4$ during a single growth run, while keeping the total flow rate of $SiCl_4$ and hydrogen constant at 500 sccm and a constant flow rate of BCl_3 at 22 sccm. The growth sequence was as follows: 1) 10 sccm $SiCl_4$ for 10 minutes (80

μm), 2) 1 sccm $SiCl_4$ for 10 minutes (1-2 μm), 3) 10 sccm $SiCl_4$ for 10 minutes (80 μm). The number of facets changed from 12 to 6 to 12 when the flow rate of $SiCl_4$ was changed from 10 to 1 to 10 sccm, as shown in Figure 4-9. This observation was consistent with the number of facets observed in microwires grown at 10 and 1 sccm of $SiCl_4$ flow rate.

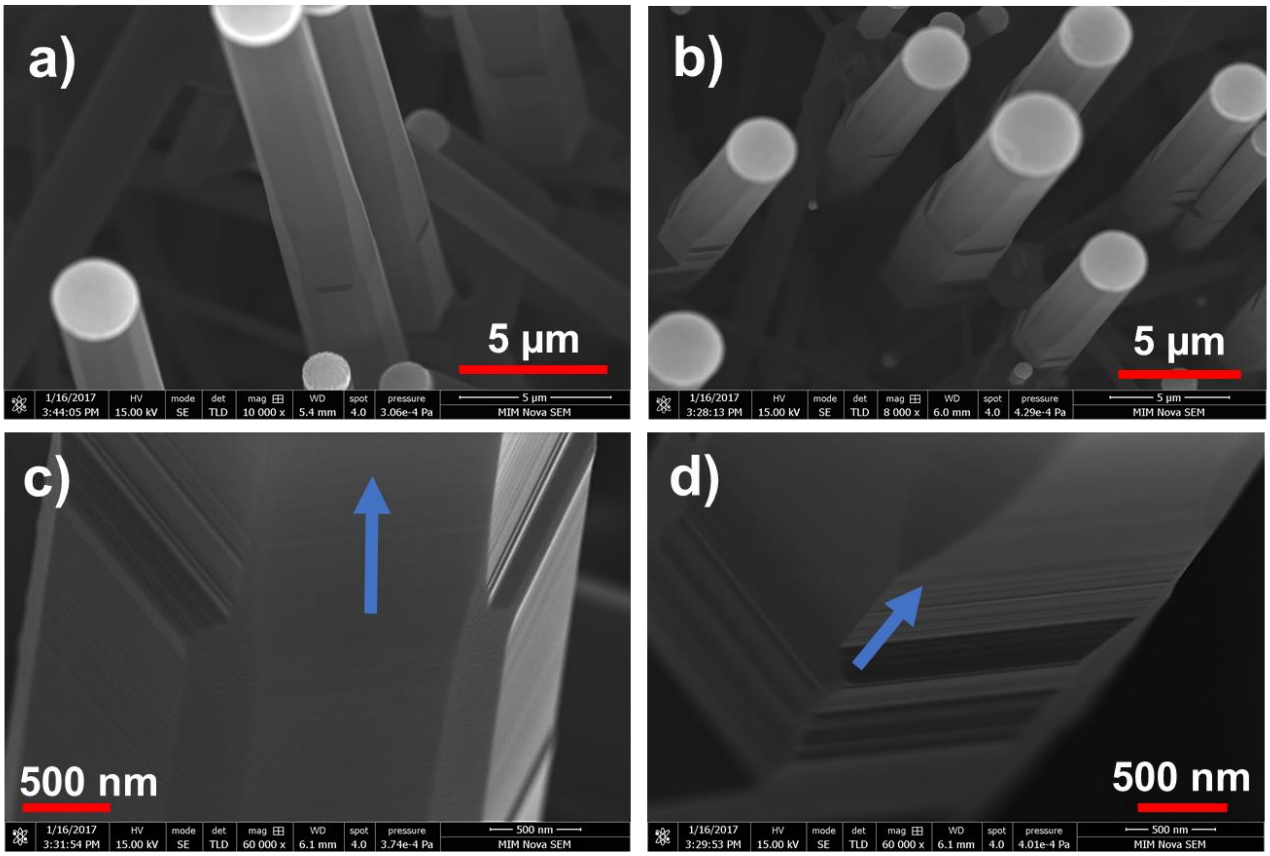

Figure 4-9 Composite Si microwires - $SiCl_4$ flow rate of 10/1/10 sccm. a) & b) evidence of 12-faceted wire grown at 10 sccm with transition to a 6-faceted wire grown during 1 sccm growth. c) & d) detail of transition between 12- and 6- faceted growth mode (arrows pointing the transitions).

Two-point electrical measurements were done on these wires from end to end and at one end of the wire (10 sccm $SiCl_4$ flow rate region) as shown in Figure 4-10a and 4-10b respectively. The resistance calculations showed that the region where the transition happened (3-5 μm), has a resistance equal to the rest of the microwire. For very high currents (~9 mA) in the microwires

grown at 10 sccm or 1 sccm, the transition region melted as can be seen in Figure 4-10d. Therefore, indicating that the transition region is electrically defective. When pressure was applied using the probes, the microwires often cleaved at the transition region (at significantly lesser pressures than the normal microwires) as shown in figure 4-10c, suggesting that the region is mechanically defective.

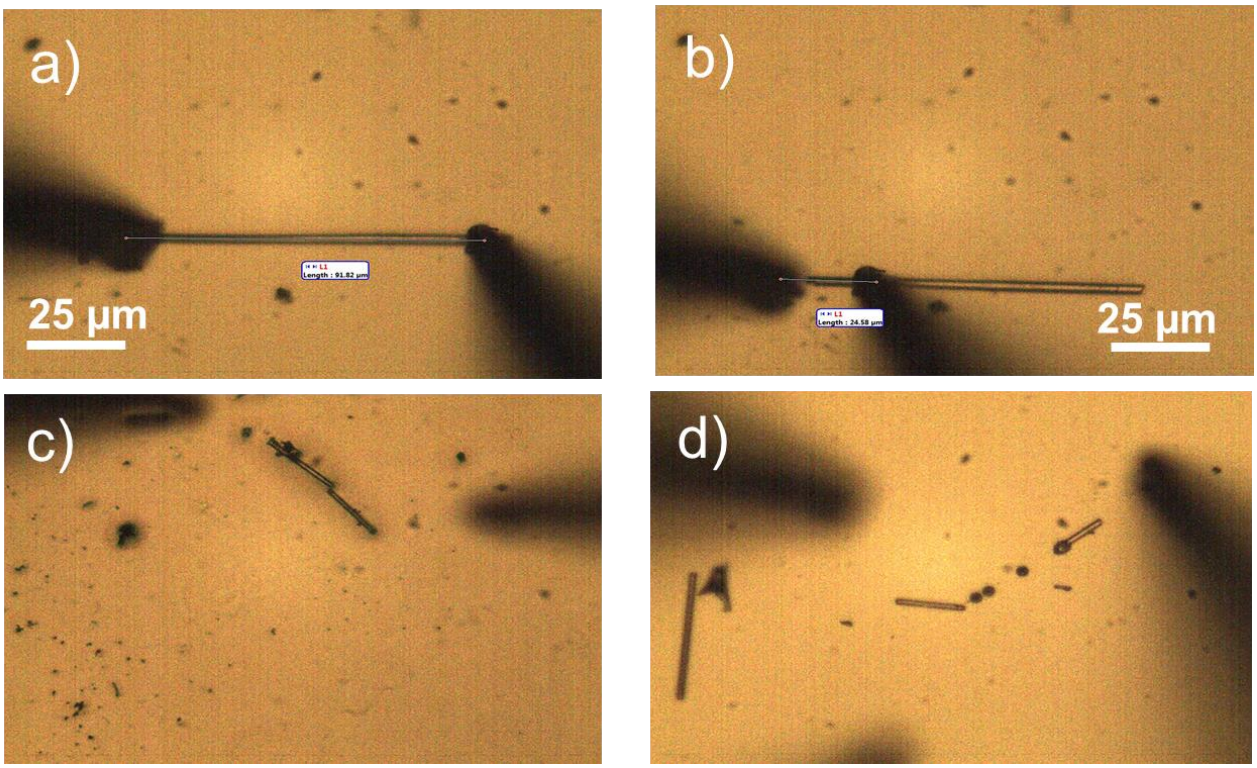

Figure 4-10 Optical images of composite Si microwires ($SiCl_4$ flow rate of 10/1/10 sccm). a) Two-point electrical measurement from end-end of wire. b) Two-point electrical measurement at one end of the wire (excluding 1 sccm-growth region). c) Wire failure (structural shear) at slow-growth region. d) wire failure (slow-growth region melting at 9 mA).

4.4 Microwire Growth at 950 ºC

As discussed above, the lower limit of doping range accessible for microwires grown at a 1000 ºC is limited by the solubility of copper. Also, changing flow rates during the growth may result in

defective microwires due to difference in sidewall deposition rates and therefore the number of facets. The sidewall growth rate was found to be directly proportional to the growth temperature. By reducing the growth temperature, the influence of sidewall deposition on the choice of flow rates for growth was minimized.

When the temperature was dropped gradually at 1 ºC/min the microwires were 12 faceted and developed sawtooth like features on the sidewalls, as reported by Ross *et al.* [81]. This effect is seen in Figure 4-11a. These features were periodic in nature and the periodicity (λ) given by λ~ 0.45R, where R is the radius of the wire [81], is in agreement with the measured periodicity of ~0.5 μm (radius = 1-1.5 μm). These features are developed because of the continuous change in the contact angle while the temperature changes gradually. When the temperature was dropped to 950 ºC suddenly, the microwires were 12 faceted with smooth sidewalls as shown in Figure 4-11b. The wire might have developed sawtooth like features but the region with such features would be very small compared to the rest of the microwire. This is a result of the cooling taking place for very short period compared to the total growth time of the wire.

Four-point measurements were done on the wires grown at 950 ºC while flowing 22 sccm BCl_3 and 10 sccm $SiCl_4$ (similar flow rates as p4) for both cooling conditions. The microwires grown with rapid cooling to 950 ºC had a doping concentration of 6.8×10^{18} cm^{-3} and the ones with gradual cooling at 1 ºC/min had a doping density of 8.5×10^{18} cm^{-3} in comparison to a doping concentration of 5.8×10^{18} cm^{-3} for microwires grown with same flow rates at 1000 ºC. Ross *et al.* associated the relatively higher value of doping concentration in the case of gradual cooling to modifications of the mobility derived from the same growth conditions that yielded sawtooth features [81].

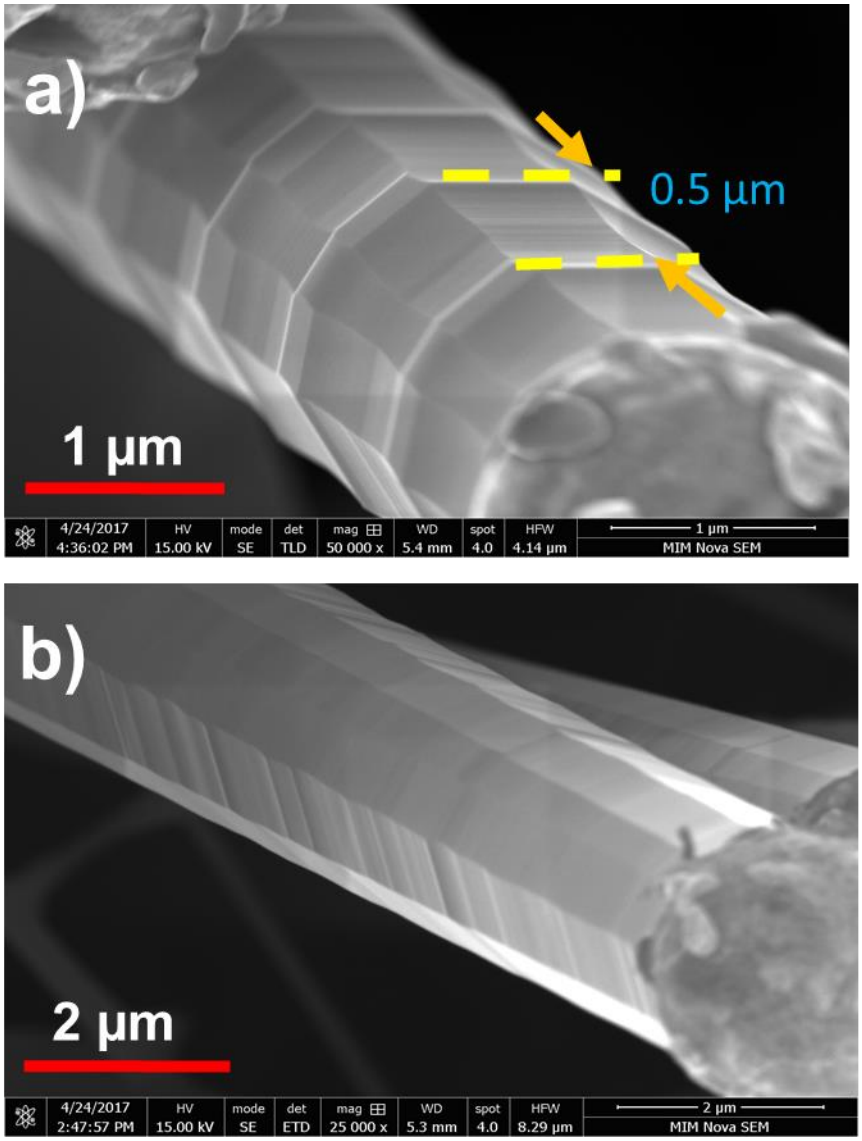

Figure 4-11 SEM images of wires grown at 950 ºC a) temperature changed at 1 ºC/min. The sidewalls are 12-faceted with saw tooth like features on the sidewalls with a periodicity of 0.5 µm. b) temperature changed by changing the set point to 950 ºC (cooling time ~ 5 minutes). The sidewalls are 12-faceted and smooth.

4.5 Intrinsic-p^+ doped microwires

Intrinsic-p^+ doped microwires were fabricated by first growing the intrinsic region with a $SiCl_4$ flow rate of 10 sccm for 15 minutes, without any dopant gas. This was followed by growing the p^+ region for 10 minutes with flow rates of 10 sccm and 22 sccm for the $SiCl_4$ and BCl_3

respectively. Based on the dependence of growth properties on precursor gas flow rates, the flow rates were chosen to grow the intrinsic-p^+ wires such that defect free microwires were produced (no signatures detected on the sidewalls or no unusual response in electrical characterizations).

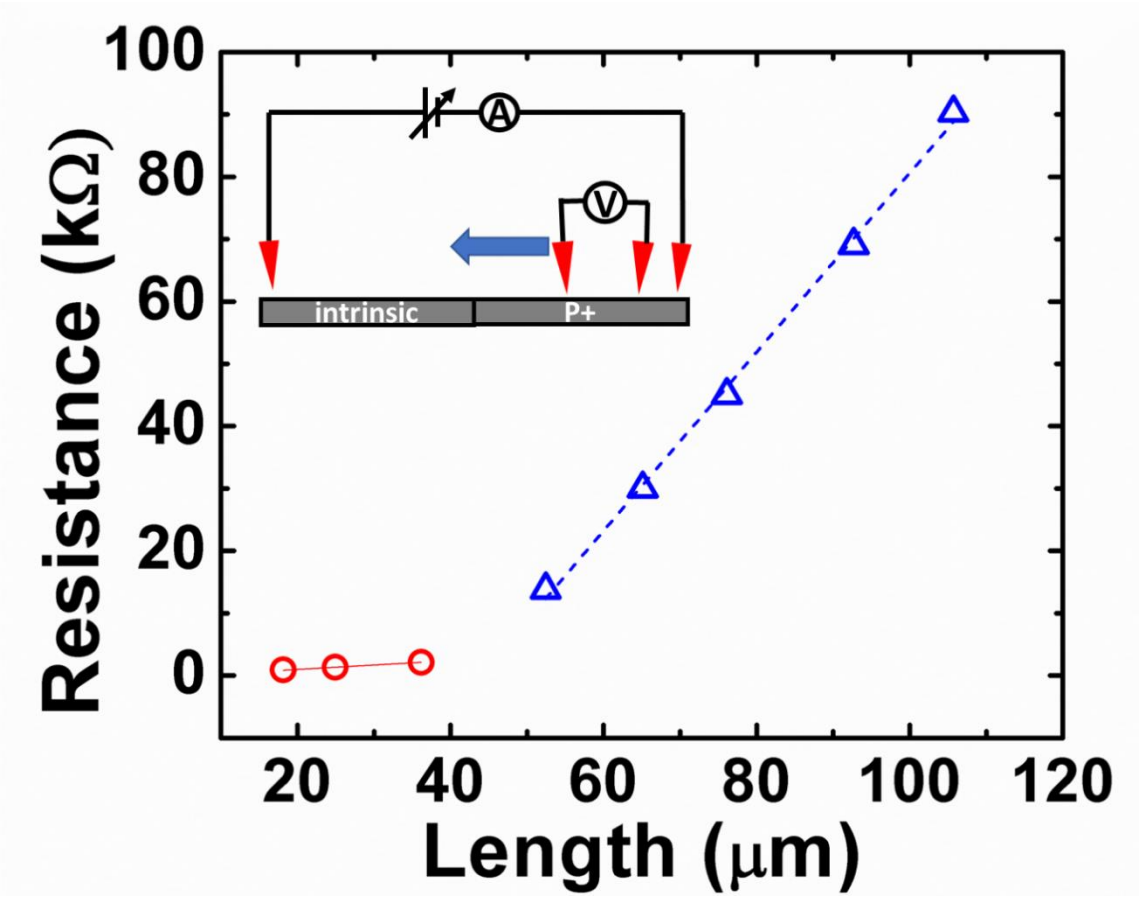

Figure 4-12 Resistance calculated from four-point measurements for different spacing between the inner probes. Inset shows the initial position of two inner probes on the p+ side and the left probe is moved in the direction of the arrow.

Four-point electrical measurements were performed on these microwires by placing the outer contacts at the ends of the microwire and measuring resistance as a function of the distance between the inner probes. The inner probes were first placed on the p^+ side and the left inner probe was moved in the direction indicated by the arrow in inset of Figure 4-12. It should be noted that

there is a sudden change in the slope of resistance curves in the graph, indicating that the probe has entered the high resistance region (intrinsic side). In this regime the resistance scales linearly with probe separation length as shown in Figure 4-12. Once, the inner probes were at maximum distance, the left inner probe was held constant and the right probe was moved in the direction indicated by the arrow in the inset of Figure 4-13. Similar behavior in the resistance vs length was seen with two differently sloped regions.

The resistivities of the p^+ section and the intrinsic section correspond to doping concentrations of 5×10^{18} cm^{-3} and $\sim 2 \times 10^{16}$ cm^{-3} respectively. The presence of a doping concentration as high as 10^{16} cm^{-3} in the intrinsic region is observed because of the doping due to the copper catalyst. The p^+ region which has the same doping conditions as p4 has a doping density similar to that of p4. It has also been observed that the transition from intrinsic to p^+ region was abrupt, which is a favorable and demonstrates the control with which the doping of the microwires could be varied. The measurement of spatial abruptness is bounded below by the size of the probes and ability to measure distances.

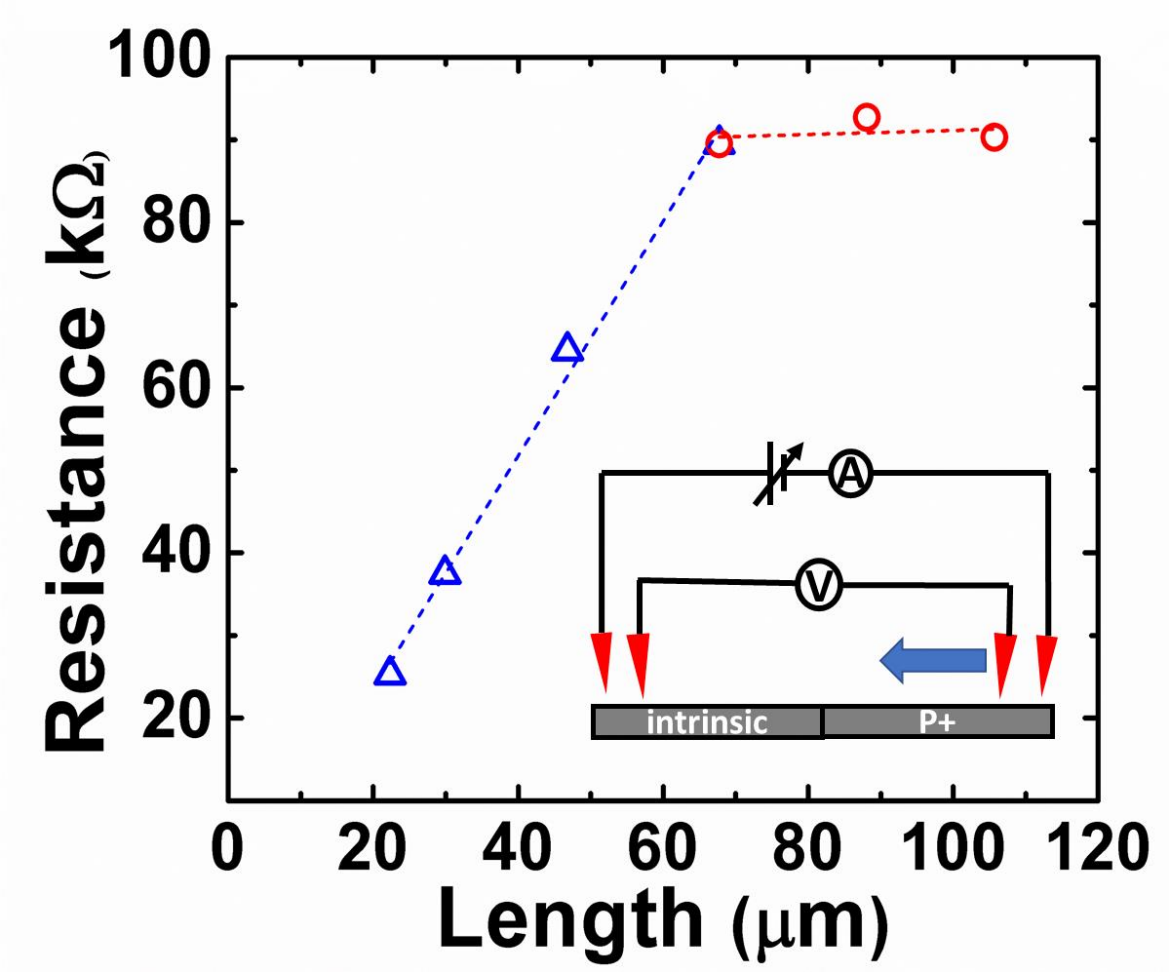

Figure 4-13 Resistance calculated from four-point measurements for different spacing between the inner probes. Inset shows the initial position of two inner probes, one on the intrinsic and other on the p^+ side and the right probe is moved in the direction of the arrow.

5 Conclusions and Future work

5.1 Conclusions

An artificial photosynthesis device was envisaged by Gray [10] which would use sunlight to split water into hydrogen and oxygen. The hydrogen gas could then be used as fuel. The prototype proposed by Gray has arrays of microwires, doped as p-type to drive the hydrogen evolution reaction (HER) at the cathode and n-type to drive the oxygen evolution reaction (OER) at the anode. The arrays of microwires are supported by a membrane which is transparent, allows the exchange of protons across the membrane and separates the reaction products (oxygen and hydrogen). The energy gap between the conduction and valence band of the semiconductor used to carry out the water splitting reaction which was required to straddle the electrochemical potentials driving the HER and OER. To implement such a device using silicon as the semiconductor material, a dual band gap structure was proposed using a p-i-n structure where the doping levels of the p and n-side chosen are such that the energy gap between conduction band on the HER side and valence band on the OER side is greater than 1.23 eV. The practical value to effectively drive the water splitting reaction is 1.6-2.4 eV. For effective carrier collection and to minimize ohmic losses in the device, the semiconductor arrays need to defect free. In addition to the energy requirements for the semiconductors, catalysts were attached to the surface of the semiconductor for the efficient transfer of carriers at the semiconductor/electrolyte junction. The VLS method was used to grow microwire arrays, using copper as the metal catalyst. In this study an investigation the influence of the silicon precursor gases and the dopant gases flow rates on the electrical and morphological properties of the microwires was undertaken.

The silicon microwire growth rates were found to be proportional to the flow rate of the $SiCl_4$ precursor gas. Four-point electrical measurements were used to calculate the doping

concentrations of the microwires. The n-type nature of the copper catalyst which gets incorporated into the microwires during growth was confirmed. It was also observed that the solubility of copper in silicon limits the minimum doping levels for both p and n-type microwires. The minimum doping concentration of both the p and the n-type microwires were decreased due to the presence of the Cu. When the doping concentration is orders higher than the solubility of copper, both p and n-type microwire doping concentrations showed similar dependence on the volume fraction of the dopant gas. The n-type doping concentrations were varied from 1.1×10^{17} cm^{-3} to 2.9×10^{19} cm^{-3} as the volume fraction was increased from 50 to 1000 ppm. The p-type doping concentrations varied from 5.5×10^{18} cm^{-3} to 9.2×10^{19} cm^{-3} when the volume fraction was changed from 2000 to 40000 ppm. For volume fractions below 2000 ppm, the p-type doping concentrations are comparable to the solubility of copper and measured doping concentration in such microwires represents the net doping density.

The sidewall of the microwires had faceting due to the radial growth which occurred at a rate two orders lower than the axial growth. When the microwires were grown at higher flow rates of $SiCl_4$, they were 12-faceted, known to be with alternating {211} and {110} facets [35]. But when the microwires were grown at a lower flow rate they were 6-faceted (all {211} facets) [35]. The chloride atoms from the $SiCl_4$ passivate the silicon atoms on the sidewalls. At lower concentrations of $SiCl_4$, the chloride density on the sidewalls passivating the microwire surface is reduced which results in less sidewall deposition rate is reduced and as the wire grows slowly, the sidewalls are exposed to sidewall deposition for longer durations. When the sidewall deposition rate increases, the {110} facet is more prone to deposition. When the flow rate of $SiCl_4$ is changed from 10 to 1 and then back to 10 sccm during a single growth, the sidewall of the microwire changed from 12 to 6 to 12-faceted. The transition region was found to be electrically and mechanically defective.

As such it is not recommended that flow rates be changed without considering its effect on the physical and electrical properties of the resultant microwires.

When the microwires were grown for 6 hours, the sidewalls are exposed to deposition resulting in almost triangular shaped microwires. The dopant atoms also play a role in determining the sidewall properties of the microwires. At higher boron concentrations in the reaction chamber, there is an increased sidewall deposition due to the acceptor nature of the boron atoms [77]. It was also observed that with a decrease in the concentration of phosphorus in the reaction chamber, there is an increased sidewall deposition due to the donor nature of phosphorus atom [80].

As the sidewall deposition reduces with a decrease in temperature, microwires were grown at 950 ºC by saturating the droplet at 1000 ºC and dropping the temperature. The sidewall developed sawtooth like features with a periodicity of ~0.5 µm when the temperature was dropped at 1 ºC/min and these microwires showed slightly higher doping concentrations because of the implications of the sawtooth features on the mobility. When the temperature was dropped suddenly from 1000 ºC to 950 ºC, the sidewalls were smooth and 12-faceted, and the doping changed by about 15% compared to wires grown under same conditions at 1000 ºC. Intrinsic-p+ microwires were grown and the flow rates were changed in way to grow defect free microwires. An abrupt (~5-10 µm) junction (within the spatial ability of the probes) was observed at the transition.

5.2 Future Work

The dopant atoms have an ability to show residual doping effects even after turning off the dopant gas leading to decreasing doping concentration over a wide region. For the artificial photosynthetic device described in this work, it is necessary to grow a p-i-n microwire with an abrupt transition between the regions. The abruptness depends on the solubility and segregation coefficients of the dopant atoms. To understand the abruptness of the transition between differently doped regions,

intrinsic-p^+ wires were grown. It was observed that the dopants started to get incorporated immediately when the BCl_3 gas was flowed into the reaction chamber. The next step would be growing p^+-intrinsic microwires and study the nature of the transition region. A similar study needs to be done on intrinsic-n^+ and n^+-intrinsic microwires.

The segregation coefficient of phosphorus atom in silicon is higher than that of boron, so it is expected that the transition region in n^+-intrinsic would be more abrupt than the p^+-intrinsic sample. Based on the results of such a study, n-i-p microwires it should be possible to obtain more abrupt interfaces at each of the transition.

The efficiency of catalyst attachment to the sidewalls needs to be studied as well for both 6 and 12-faceted microwires. The flow rates can be chosen accordingly during growth depending on the number of facets that are favorable.

6 Appendix A

Calibration of the temperature in the furnace

The substrates were placed 6-10 cm away from the center, on the side from which the gases enter, to obtain uniform growth across their entire area. The temperature profile inside the furnace needs to be understood to know the gap between the temperature setpoint and the temperature at the position of the substrate. The temperature at different points inside the quartz tube was measured by opening it on both sides. The temperature of the furnace was set to 300, 500, 1000 ºC and waited till the reading on the furnace display reached the setpoint. A thermo-couple (Omega Part # Bare-20-K-12 AC#PL 2009/05) was inserted from one side and the other end was connected to a multimeter that displayed the temperature corresponding to the potential difference generated between the ends of the thermocouple. The tip of the thermocouple was held in position and waited till the temperature reading settled and that number was recorded.

The thermo-couple had ceramic separators (alternate 1, 1.5 cm long) at equal intervals which were used as a reference for the position of the tip of the thermo-couple. It was observed that in the region where the substrates are placed the temperature is ~5% lower than the setpoint (figure 6-1). But when the actual growth is happening the quartz tube is sealed and the airflow is expected to be lower than 5%. Growth was not observed when the substrates were placed 6-10 cm on the side the gases exit and silicon coating on the inside of the quartz tube happened at 6-10 cm on the entry side of the gases. The reason could be related to the direction of air currents inside the tube during the growth and also it is expected that the temperature profile is not symmetric on either side of the center of the furnace.

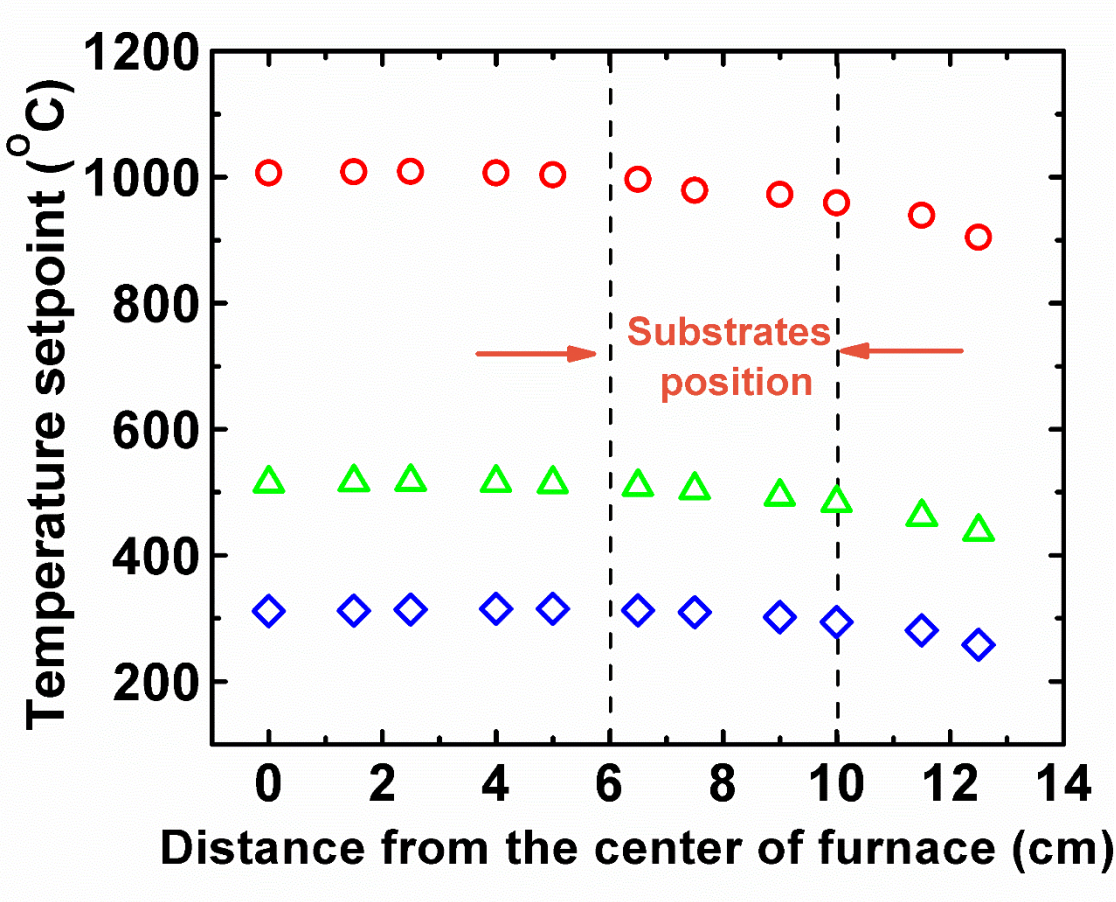

Figure 6-1 Temperature profile inside the furnace as a function of distance from the center on the entry side of the gases. The region where substrates are placed is marked in the figure.

7 Appendix B

Volume fraction calculation

The $SiCl_4$ is inside a 1-liter steel bubbler containing 500 g of $SiCl_4$. The volume occupied by 500 g of $SiCl_4$ is given by:

$$V = m/\rho$$

where ρ is the density of $SiCl_4$ (1.483 g/ml) and m is the mass of $SiCl_4$. The 500 g of $SiCl_4$ occupies a volume of 337.15 ml and the headspace in the tank is 1000-337.15=662.85 ml. Vapor of $SiCl_4$ is present above the liquid and there exists an equilibrium between them. The number of moles of $SiCl_4$ in vapor phase is given by:

$$n = \frac{P_{vap}V}{RT}$$

where P is the vapor pressure of $SiCl_4$ at 300 K (34kPa), V is the volume of $SiCl_4$, R is the universal gas constant and T is the temperature (in K). The number of moles from this calculation is 4.5956 millimoles. The concentration of vapor in the headspace (c) is given by:

$$c = \frac{n}{V_{headspace}} = 6.933\ \mu mol/ml$$

Hydrogen gas is bubbled through the $SiCl_4$ tank to transport $SiCl_4$ to the reaction chamber. A flowrate of *f* sccm hydrogen is equal to *f* ml/min. The moles of $SiCl_4$ carried by the hydrogen per minute is given by $c \times f$ which is equal to 6.933*f* μmol/min, which corresponds to a volume of

$$V = 6.933f\,\frac{\mu mol}{ml} \times 22400\,\frac{ml}{mol} \times \frac{300}{273} = 0.17f\ ml/min$$

The p-type doping source, boron trichloride gas is diluted in hydrogen and the concentration is 250 ppm BCl_3 and the n-type doping source, phosphine gas is diluted in hydrogen and the concentration is 100 ppm PH_3 in hydrogen. For flowrate of f_p sccm for BCl_3 and f_n sccm for PH_3 their actual flowrate is given as:

$$for\ BCl_3: \frac{250}{10^6} \times f_p\ ml/min$$

$$for\ PH_3: \frac{100}{10^6} \times f_n\ ml/min$$

The volume fraction (in ppm) is the ratio of actual flowrate of dopant gas to actual flowrate of $SiCl_4$ and is given by:

$$for\ BCl_3: \frac{\frac{250}{10^6} \times f_p\ ml/min}{0.17f\ ml/min} = 1470.59\frac{f_p}{f}\ ppm$$

$$for\ PH_3: \frac{\frac{100}{10^6} \times f_p\ ml/min}{0.17f\ ml/min} = 588.24\frac{f_p}{f}\ ppm$$

8 Appendix C

Etching using KOH to identify differently doped regions

KOH solution etches silicon at different rates based on the doping levels and type of doping of the silicon and KOH of silicon microwires was used to demonstrate differently doped regions in a silicon nanowire [82]. To understand the extent of reservoir effect for the growth conditions used in this study, intrinsic and p-type doped wires etched to see the effect. Intrinsic wires were grown at 10 sccm $SiCl_4$ flowrate and the axial growth direction being <111>. Each etch was done using 30% KOH solution at 80 ºC for 15 minutes. The etch rate in <111> direction is ~0.96 μm/hr). All the microwires were etched away (Figure 9-1) demonstrating that <111> is not the etch direction and <110> could be a possible etch direction (6 facets in a 12-faceted microwire has this orientation) which has an etch rate of ~121 μm/hr for the same conditions.

Due to the high etch rates for the 12-faceted intrinsic wires, p-type doped wires grown by flowing 10 sccm of $SiCl_4$ and 22 sccm of BCl_3 was used (doped wires have lowered etch rates in KOH). In addition to choosing doped microwires the temperature and etch time was reduced to 50 ºC and 210 seconds respectively. It was observed that the microwires became thinner and the thickness changed from ~ 3 μm to ~ 0.8 μm (figure 8-2) and this change is close to the etch rate of <110> direction for the conditions used (18.99 μm/hr). As the KOH etching of the microwires grown in this study needed a standardized recipe and is a time taking process, this direction was not pursued for longer time. But from these initial experiments, it is predicted that the KOH etch rate in <110> direction is the key to developing a recipe for such an etch.

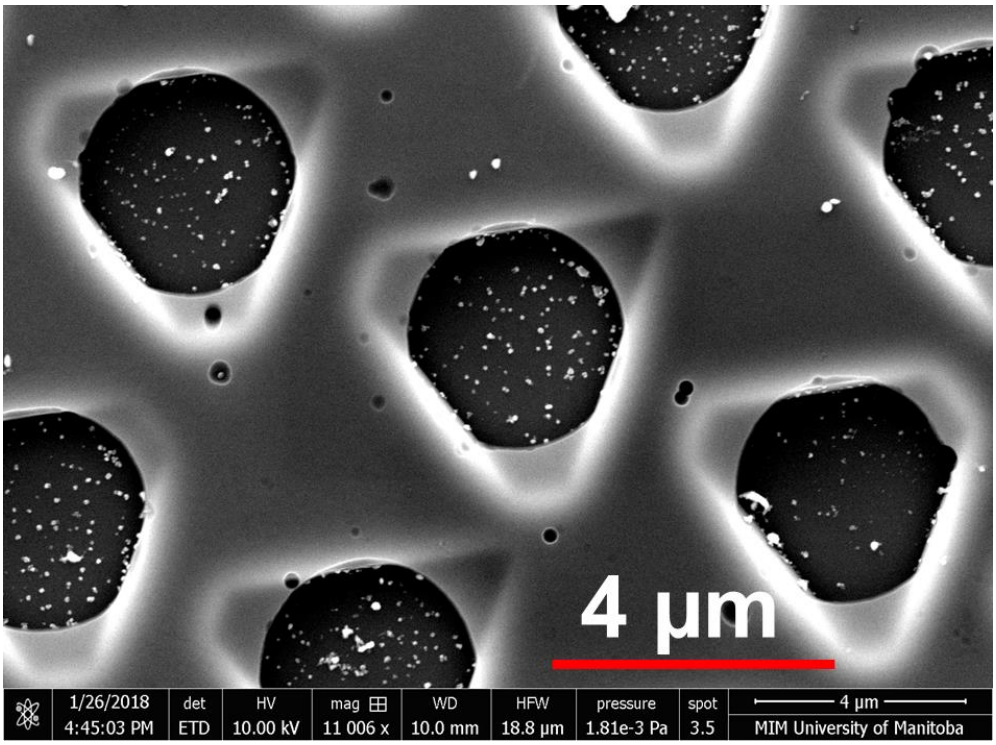

Figure 8-1 Substrate surface completely etched after 15 minutes etch in KOH at 80 ºC

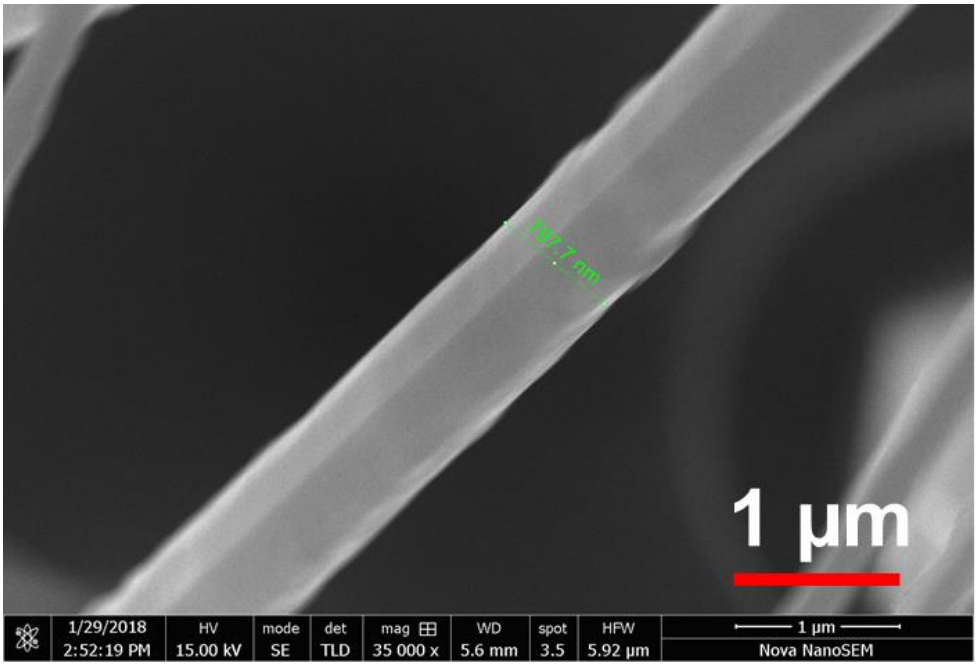

Figure 8-2 SEM image of a p-type microwire etched for 210 seconds in KOH at 50 ºC and thickness changed from ~ 3 µm to ~ 0.8 µm (marked in the figure).

9 Appendix D

Transmission Electron Microscope (TEM) imaging of the microwires

The microwires grown in this study have a diameter of ~ 3 μm. To image a sample using TEM the sample should be transparent to the electrons and the thicknesses of the wires is significantly higher to study in a TEM. The thickness of the microwires was reduced by ion milling machining. The microwires were transferred to a TEM grid using the same technique used to prepare slide for electrical measurements. The grid was placed under the optical microscope and probes were used to move the microwires onto the grid as shown in Figure 9-1.

The wires were imaged using TEM (FEI Talos F200X) and the microwires clearly were transparent to the electron beam and imaging was possible (Figure 9-2). But the milling process damaged the microwire surface to prevent the observation of crystal directions clearly.

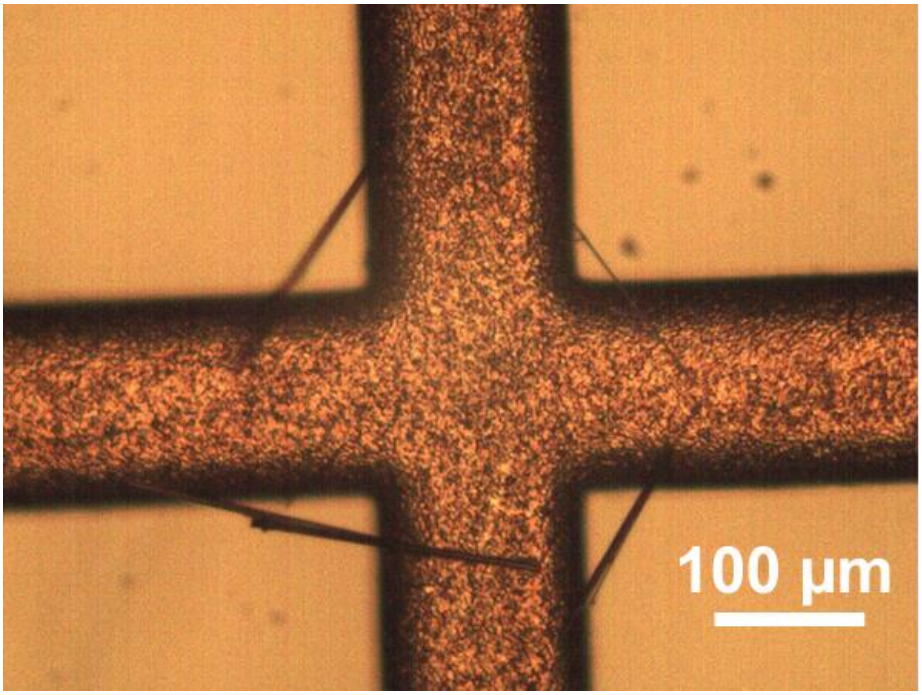

Figure 9-1 TEM grid with microwires placed on the grid.

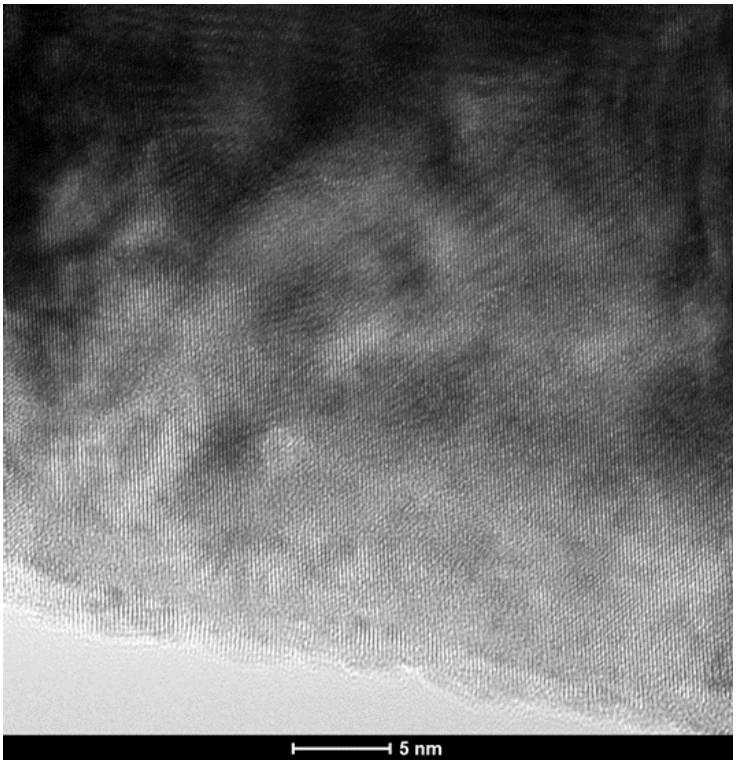

Figure 9-2 TEM image of the ion milled microwires.

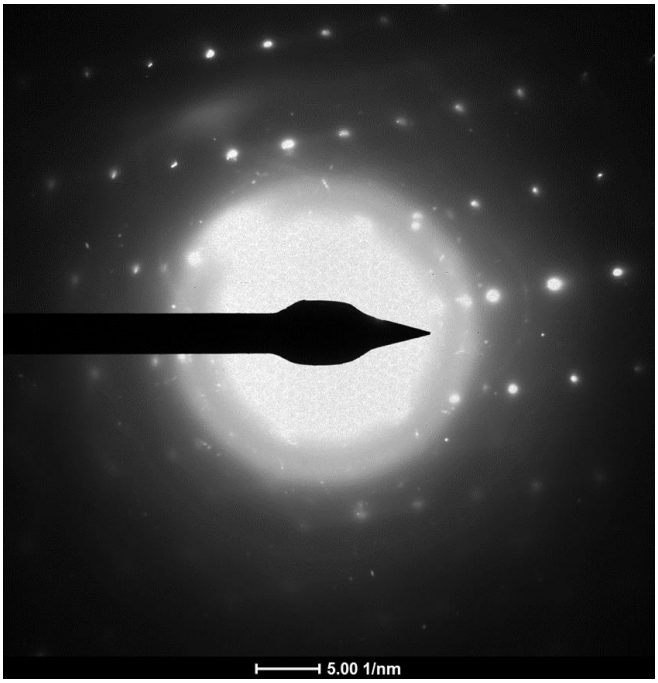

Figure 9-3 Diffraction pattern of the microwire. The bright spot is due to the amorphous layer of silicon that is present because of the milling.

10 References

[1] https://www.un.org/development/desa/publications/world-population-prospects-the-2017-revision.html.

[2] M. G. Walter *et al.*, “Solar Water Splitting Cells.,” *Chem. Rev. (Washington, DC, United States)*, vol. 110, no. 11, pp. 6446–6473, 2010.

[3] A. Fujishima and K. Honda, "Electrochemical Photolysis of Water at a Semiconductor Electrode", *Nature*, vol. 238, pp. 37-38, 1972.

[4] W. Shockley and H. J. Queisser, “Detailed Balance Limit of Efficiency of p-n Junction Solar Cells,” *J. Appl. Phys.*, vol. 32, no. 3, pp. 510-519, 1961.

[5] A. J. Bard and M. A. Fox, “Photosynthesis : Solar Splitting of Water to Hydrogen and Oxygen,” *Acc. Chem. Res.*, vol. 28, pp. 141–145, 1995.

[6] B. M. Kayes, H. A. Atwater, N. S. Lewis, “Comparison of the device physics principles of planar and radial p-n junction nanorod solar cells,” *J. Appl. Phys.*, vol. 97, pp. 114302, 2005.

[7] J. R. Maiolo, H. A. Atwater, and N. S. Lewis, “Macroporous Silicon as a Model for Silicon Wire Array Solar Cells,” *J. Phys. Chem. C*, vol. 112, pp. 6194–6201, 2008.

[8] J. R. Bolton, S. J. Strickler and J. S. Connolly, "Limiting and realizable efficiencies of solar photolysis of water," *Nature*, vol. 316, no. 8, pp. 495-500, 1985.

[9] J. A. Turner, “A Realizable Renewable Energy Future,” *Science*, vol. 285, pp. 687–689, 1999.

[10] H. B. Gray, “Powering the planet with solar fuel,” *Nat. Chem.*, vol. 1, p. 7, 2009.

[11] R. S. Wagner and W. C. Ellis, “Vapor-liquid-solid mechanism of single crystal growth,” *Appl. Phys. Lett.*, vol. 4, no. 5, pp. 89–90, 1964.

[12] E. I. Givargizov, “Fundamental aspects of VLS growth,” *J. Cryst. Growth*, vol. 31, pp. 20–30, 1975.

[13] G. A. Bootsma and H. J. Gassen, “A quantitative study on the growth of silicon whiskers from silane and germanium whiskers from germane,” *J. Cryst. Growth*, vol. 10, pp. 223–234, 1971.

[14] V. Schmidt, J. V. Wittemann, S. Senz, and U. Gosele, “Silicon nanowires: A review on aspects of their growth and their electrical properties,” *Adv. Mater.*, vol. 21, pp. 2681–2702, 2009.

[15] H. Baker, *Alloy Phase Diagrams*. ASM International, 1992.

[16] Gyu-Chul Yi, *Semiconductor Nanostructures for Optoelectronic Devices*. Springer- Verlag Berlin Heidelberg, 2012.

[17] V. A. Nebol’sin and A. Shchetinin, “Role of surface energy in the vapor–liquid–solid growth of silicon,” *Inorg. Mater.*, vol. 39, no. 9, pp. 899–903, 2003.

[18] B. M. Kayes, *et al.*, “Growth of vertically aligned Si wire arrays over large areas (>1 cm2) with Au and Cu catalysts,” *Appl. Phys. Lett.*, vol. 91, p. 103110, 2007.

[19] V. Ganapati *et al.*, “Seeding of silicon wire growth by out-diffused metal precipitates,” *Small*, vol. 7, no. 5, pp. 563–567, 2011.

[20] J. Arbiol *et al.*, “Influence of Cu as a catalyst on the properties of silicon nanowires synthesized by the vapour–solid–solid mechanism,” *Nanotechnology*, vol. 18, p. 305606,

2007.

[21] Y. Wang, V. Schmidt, S. Senz, and U. Gösele, “Epitaxial growth of silicon nanowires using an aluminium catalyst,” *Nat. Nanotechnol.*, vol. 1, pp. 186–189, 2006.

[22] Y. Ke *et al.*, “Fabrication and Electrical Properties of Si Nanowires Synthesized by Al Catalyzed Vapor-Liquid-Solid Growth,” *Nano Lett.*, vol. 9, no. 12, pp. 4494–4499, 2009.

[23] M. Dutta *et al.*, “Diameter-controlled growth and impurity doping of silver colloid-seeded silicon microwires to nanowires for the realization of solar cell materials,” *Mater. Express*, vol. 3, no. 1, pp. 85–91, 2013.

[24] H. Fang, Y. Wu, J. Zhao, and J. Zhu, “Silver catalysis in the fabrication of silicon nanowire arrays,” *Nanotechnology*, vol. 17, pp. 3768–3774, 2006.

[25] J. V. Wittemann *et al.*, “Silver catalyzed ultrathin silicon nanowires grown by low-temperature chemical-vapor-deposition,” *J. Appl. Phys.*, vol. 107, p. 096105, 2010.

[26] V. A. Nebol’sin *et al.*, “Effect of the nature of the metal solvent on the vapor-liquid-solid growth rate of silicon whiskers,” *Inorg. Mater.*, vol. 41, no. 12, pp. 1256–1259, 2005.

[27] D. W. F. James and C. Lewis, “Silicon Whisker Growth and Epitaxy By the Vapour-Liquid-Solid Mechanism,” *Brit. J. Appl. Phys.* vol. 16, pp. 1089-1094, 1965.

[28] J. Weyher, “Some notes on the growth kinetics and morphology of VLS silicon crystals grown with platinum and gold as liquid-forming agents,” *J. Cryst. Growth*, vol. 43, pp. 235–244, 1978.

[29] S.-W. Chung, J.-Y. Yu, and J. R. Heath, “Silicon nanowire devices,” *Appl. Phys. Lett.*, vol. 76, no. 15, pp. 2068–2070, 2000.

[30] M. Demeri, M. Farag, and J. Heasley, “Surface tension of liquid Pb-Sn alloys,” *J. Mat. Sci.*, vol. 9, pp. 683-685, 1974.

[31] W. Gąsior, Z. Moser, and J. Pstruś, “Surface Tension, Density, and Molar Volume of Liquid Sb-Sn Alloys: Experiment Versus Modeling,” *J. Phase Equilibria*, vol. 24, no. 6, pp. 504–510, 2003.

[32] S. Amore, E. Ricci, T. Lanata, and R. Novakovic, “Surface tension and wetting behaviour of molten Cu-Sn alloys,” *J. Alloys Compd.*, vol. 452, no. 1, pp. 161–166, 2003.

[33] F. Iacopi *et al.*, “Plasma-enhanced chemical vapour deposition growth of Si nanowires with low melting point metal catalysts: An effective alternative to Au-mediated growth,” *Nanotechnology*, vol. 18, p. 505307, 2007.

[34] E. I. Givargizov and N. N. Sheftal’, “Morphology of silicon whiskers grown by the VLS-technique,” *J. Cryst. Growth*, vol. 9, pp. 326–329, 1971.

[35] R. S. Wagner and C. J. Doherty, “Controlled Vapor-Liquid-Solid Growth of Silicon Crystals,” *J. Electrochem. Soc.*, vol. 113, no. 12, pp. 1300–1305, 1966.

[36] E. I. Givargizov, *Highly Anisotropic Crystals*. Springer Netherlands, 1987.

[37] B. Ressel *et al.*, “Wetting of Si surfaces by Au – Si liquid alloys,” vol. 93, no. 7, pp. 3886-3892, 2003.

[38] S. Kodambaka *et al.*, “Diameter-independent kinetics in the vapor-liquid-solid growth of Si nanowires,” *Phys. Rev. Lett.*, vol. 96, p. 096105, 2006.

[39] V. Schmidt, S. Senz, and U. Gosele, “The shape of epitaxially grown silicon nanowires and the influence of line tension,” *Appl. Phys. A.*, vol. 80, pp. 445–450, 2005.

[40] A. B. Greytak *et al.*, "Growth and transport properties of complementary germanium nanowire field-effect transistors," *Appl. Phys. Lett.*, vol. 84, no. 21, pp. 4176–4178, 2004.

[41] D. Wang *et al.*, "Germanium nanowire field-effect transistors with SiO_2 and high-κ HfO_2 gate dielectrics," *Appl. Phys. Lett.*, vol. 83, no. 12, pp. 2432–2434, 2003.

[42] Y. Wu *et al.*, "Controlled growth and structures of molecular-scale silicon nanowires," *Nano Lett.*, vol. 4, no. 3, pp. 433–436, 2004.

[43] M. Yamanaka, I. Sakata, and T. Sekigawa, "Effects of film quality of hydrogenated amorphous silicon grown by thermal chemical-vapor-depositon on subsequent in-situ hydrogenation processes," *Jpn. J. Appl. Phys.*, vol. 39, no. 6A, pp. 3302–3307, 2000.

[44] J. Kikkawa, Y. Ohno, and S. Takeda, "Growth rate of silicon nanowires," *Appl. Phys. Lett.*, vol. 86, p. 123109, 2005.

[45] K. K. Lew and J. M. Redwing, "Growth characteristics of silicon nanowires synthesized by vapor-liquid-solid growth in nanoporous alumina templates," *J. Cryst. Growth*, vol. 254, pp. 14–22, 2003.

[46] W. H. Shepherd, "Vapor Phase Deposition and Etching of Silicon," *J. Electrochem. Soc.*, vol. 112, no. 10, pp. 988–994, 1965.

[47] F. Dhalluin *et al.*, "Critical condition for growth of silicon nanowires," *J. Appl. Phys.*, vol. 102, p. 094906, 2007.

[48] L. Schubert *et al.*, "Silicon nanowhiskers grown on 〈111〉 Si substrates by molecular-beam epitaxy," *Appl. Phys. Lett.*, vol. 84, no. 24, pp. 4968–4970, 2004.

[49] J. Wallentin and M. T. Borgström, "Doping of semiconductor nanowires," *J. Mater. Res.*,

vol. 26, no. 17, pp. 2142–2156, 2011.

[50] H. Schmid *et al.*, "Doping Limits of Grown in situ Doped Silicon Nanowires Using Phosphine," *Nano Lett.*, vol. 9, no. 1, pp. 173-177, 2009.

[51] E. I. Givargizov, "Periodic instability in whisker growth," *J. Cryst. Growth*, vol. 20, pp. 217–226, 1973.

[52] F. Li, P. D. Nellist, and D. J. H. Cockayne, "Doping-dependent nanofaceting on silicon nanowire surfaces," *Appl. Phys. Lett.*, vol. 94, p. 263111, 2009.

[53] L. J. Lauhon *et al.*, "Epitaxial core-shell and core-multishell nanowire heterostructures," *Nature*, vol. 420, pp. 57–61, 2002.

[54] K. K. Lew *et al.*, "Structural and electrical properties of trimethylboron-doped silicon nanowires," *Appl. Phys. Lett.*, vol. 85, no. 15, pp. 3101–3103, 2004.

[55] G. Zheng *et al.*, "Synthesis and fabrication of high-performance n-type silicon nanowire transistors," *Adv. Mater.*, vol. 16, no. 21, pp. 1890–1893, 2004.

[56] P. Taylor, W. E. Spear, and P. G. Le Comber, "Electronic properties of substitutionally doped amorphous Si and Ge," no. July 2013, pp. 37–41, 2006.

[57] Y. Wang *et al.*, "Use of phosphine as an n-type dopant source for vapor-liquid-solid growth of silicon nanowires," *Nano Lett.*, vol. 5, no. 11, pp. 2139–2143, 2005.

[58] R. H. Hopkins and A. Rohatgi, "Impurity effects in silicon for high efficiency solar cells," *J. Cryst. Growth*, vol. 75, pp. 67–79, 1986.

[59] R. N. Hall, J. H. Racette, "Diffusion and Solubility of Copper in Extrinsic and Intrinsic Germanium, Silicon, and Gallium Arsenide," *J. Appl. Phys.*, vol. 35, no. 2, pp. 379-397,

1964.

[60] W. C. Dash, “Gold-induced climb of dislocations in silicon,” *J. Appl. Phys.*, vol. 31, no. 12, pp. 2275–2283, 1960.

[61] A. R. Neureuther, “The Lithography Process and Basic Simulation Models,” pp. 117–155, Springer Verlag, 2000.

[62] M. Binnewies, and K. Jug, “The Formation of a Solid from the Reaction $SiCl_4$ (g) + O_2 (g) -> SiO_2 (s) + $2Cl_2$ (g),” *Eur. J. Inorg. Chem.*, vol. 4, pp. 1127-1138, 2000.

[63] M. D. Kelzenberg *et al.*, “Photovoltaic Measurements in Single-Nanowire Silicon Solar Cells,” *Nano Lett.*, vol. 8, no. 2, pp. 710-714, 2008.

[64] I. Yahyaie *et al.*, “Electrical characterization of Si Microwires and of Si microwire/conducting polymer composite junctions,” *J. Phys. Chem. Lett.*, vol. 2, pp. 675–680, 2011.

[65] W. Paul, “Pressure Dependence of the Resistivity of Silicon,” *Phy. Rev.*, vol. 98, no. 6, pp. 1755–1757, 1955.

[66] P. W. Bridgman, “The effect of pressure on the electrical resistance of certain semi-conductors,” *Proc. of the American Academy of Arts and Sci.*, vol. 79, no. 3, pp. 127–148, 1951.

[67] J. E. Bradby and J. S. Williams, “In situ electrical characterization of phase transformations in Si during indentation,” *Phys. Rev. B*, vol. 67, p. 085205, 2003.

[68] S. Ruffell *et al.*, “Identification of nanoindentation-induced phase changes in silicon by in situ electrical characterization,” *J. Appl. Phys.*, vol. 101, p. 083531, 2007.

[69] I. Yahyaie *et al.*, "Characterization of the electrical properties of individual p-Si microwire/polymer/n-Si microwire assemblies," *J. Phys. Chem. C*, vol. 115, pp. 24945–24950, 2011.

[70] J. T. Engel *et al.*, "Direct contact four-point probe characterization of Si microwire absorbers for artificial photosynthesis," *RSC Adv.*, vol. 6, pp. 110344–110348, 2016.

[71] A. A. Istratov *et al.*, "Diffusion, solubility and gettering of copper in silicon," *Mat. Sci. & Engg. B*, vol. 72, pp. 99–104, 2000.

[72] R. Sachdeva, A. A. Istratov, and E. R. Weber, "Recombination activity of copper in silicon," *Appl. Phys. Lett.*, vol. 79, no. 18, pp. 2937-2939, 2001.

[73] M. C. Putnam *et al.*, "10 μ m minority-carrier diffusion lengths in Si wires synthesized by Cu-catalyzed vapor-liquid-solid growth," *Appl. Phys. Lett.*, vol. 95, p. 163116, 2009.

[74] W. R. Thurber, *et al.*, "The Relationship between resistivity and dopant density for phosphorus- and boron-doped silicon" NBS Publications, 1981.

[75] D. J. Chakrabarti and D. E. Laughlin, "The B-Cu System," *Bulletin of Alloy Phase Diagrams*, vol. 3, no. 1. pp. 45–48, 1982.

[76] F. Oehler *et al.*, "The importance of the radial growth in the faceting of silicon nanowires," *Nano Lett.*, vol. 10, pp. 2335–2341, 2010.

[77] M. S. Islam *et al.*, "High-yield growth of p-Si microprobe arrays by selective vapor-liquid-solid method using in situ doping and their properties," *J. Cryst. Growth*, vol. 306, pp. 276–282, 2007.

[78] T. Makino, H. Nakamura, "Resistivity changes of heavily-boron-doped CVD-prepared

polycrystalline silicon caused by thermal annealing," *Solid State Electronics*, vol. 24, pp. 49–55, 1980.

[79] F. Gao *et al.*, "Influence of phosphine flow rate on Si growth rate in gas source molecular beam epitaxy," *J. Cryst. Growth.*, vol. 220, pp. 461–465, 2000.

[80] M. S. Islam *et al.*, "Realization of in situ doped n-type and p-type Si-microprobe array by selective vapor-liquid-solid (VLS) growth method," *Japanese J. Appl. Phys.*, vol. 44, no. 4 B, pp. 2161–2165, 2005.

[81] F. M. Ross, J. Tersoff, and M. C. Reuter, "Sawtooth faceting in silicon nanowires," *Phys. Rev. Lett.*, vol. 95, p. 146104, 2005.

[82] J. D. Christesen *et al.*, "Encoding Abrupt and Uniform Dopant Pro fi les in Vapor À Liquid À Solid Nanowires by Suppressing the Reservoir Eff ect of the Liquid Catalyst," *ACS Nano*, vol. 8, no. 11, pp. 11790–11798, 2014.